

Classification: Biological Sciences – Neuroscience

Title: Hyperactive MEK1 signaling in cortical GABAergic neurons causes embryonic parvalbumin-neuron death and defects in behavioral inhibition.

Authors: Michael C. Holter¹, Lauren T. Hewitt^{1,#}, Kenji J. Nishimura^{1,#}, George R. Bjorklund¹, Shiv Shah¹, Noah R. Fry¹, Katherina P. Rees¹, Tanya A. Gupta², Carter W. Daniels^{2,†}, Guohui Li³, Steven Marsh⁴, David M. Treiman⁴, M. Foster Olive², Trent R. Anderson³, Federico Sanabria², William D. Snider⁵, Jason M. Newbern^{1,*}

Affiliations:

¹School of Life Sciences, ²Department of Psychology, Arizona State University; Tempe, AZ 85287, USA

³College of Medicine, University of Arizona; Phoenix, AZ 85004, USA

⁴Barrow Neurological Institute; Phoenix, AZ 85013, USA

⁵University of North Carolina Neuroscience Center, The University of North Carolina School of Medicine; Chapel Hill, NC, 27599, USA

[#]Present Address: Interdepartmental Neuroscience Graduate Program, University of Texas; Austin, TX, 78712, USA

[†]Present Address: Department of Psychiatry, Columbia University, New York, NY 10032, USA

*Corresponding Author address:

School of Life Sciences, PO Box 84501

Arizona State University

Tempe, AZ 85287-4501, USA

jason.newbern@asu.edu

1 **Abstract**

2 Abnormal ERK/MAPK pathway activity is an important contributor to the neuropathogenesis of
3 many disorders including Fragile X, Rett, 16p11.2 Syndromes, and the RASopathies. Individuals with these
4 syndromes often present with intellectual disability, ADHD, autism, and epilepsy. However, the
5 pathological mechanisms that underly these deficits are not fully understood. Here, we examined whether
6 hyperactivation of MEK1 signaling modifies the development of GABAergic cortical interneurons (CINs),
7 a heterogeneous population of inhibitory neurons necessary for cortical function. We show that
8 GABAergic-neuron specific MEK1 hyperactivation *in vivo* leads to increased cleaved caspase-3 labeling
9 in a subpopulation of immature neurons in the embryonic subpallium. Adult mutants displayed a significant
10 loss of mature parvalbumin-expressing (PV) CINs, but not somatostatin-expressing CINs, during postnatal
11 development and a modest reduction in perisomatic inhibitory synapse formation on excitatory neurons.
12 Surviving mutant PV-CINs maintained a typical fast-spiking phenotype and minor differences in intrinsic
13 electrophysiological properties. These changes coincided with an increased risk of seizure-like phenotypes.
14 In contrast to other mouse models of PV-CIN loss, we discovered a robust increase in the accumulation of
15 perineuronal nets, an extracellular structure thought to restrict plasticity in the developing brain. Indeed, we
16 found that mutants exhibit a significant impairment in the acquisition of a behavioral test that relies on
17 behavioral response inhibition, a process linked to ADHD-like phenotypes. Overall, our data suggests PV-
18 CIN development is particularly sensitive to hyperactive MEK1 signaling which may underlie neurological
19 deficits frequently observed in ERK/MAPK-linked syndromes.

20 **Significance Statement**

21 The RASopathies are a family of neurodevelopmental syndromes caused by mutations that lead
22 to increased RAS/RAF/MEK/ERK signaling and are associated with intellectual disability, epilepsy, and
23 ADHD. We do not fully understand how distinct neuronal subtypes are affected in these syndromes. Here,
24 we show that increased MEK signaling in developing mice promotes the embryonic death of a specific
25 subset of cortical inhibitory neurons that express parvalbumin. Surviving mutant parvalbumin neurons
26 also show significant changes in crucial maturation processes, which coincide with increased seizure
27 susceptibility and profound deficits in behavioral inhibition. These data suggest that deficits in inhibitory
28 circuit development contribute to RASopathy neuropathogenesis and indicate that therapeutic strategies
29 targeting inhibitory interneuron dysfunction may be beneficial for these individuals.

30

31

32

33 **Keywords**

34 ERK1/2, cerebral cortex, development, ganglionic eminence, ADHD, RASopathy, kinase, apoptosis,
35 response inhibition capacity

36 **Introduction**

37 Multiple developmental disorders are caused by genetic mutations linked to perturbation of kinase
38 activity and altered intracellular signaling. The RAS/RAF/MEK/ERK (ERK/MAPK) pathway is a well-
39 known, ubiquitous signaling cascade that is dynamically activated during development (Krens et al., 2006;
40 Samuels et al., 2009). Mutations in classic RAS/MAPK signaling pathway components or upstream
41 regulators, such as *PTPN11/SHP2*, *NF1*, or *SYNGAP1*, cause a family of related syndromes, known
42 collectively as the RASopathies (Tidyman and Rauen, 2016). Moreover, *MAPK3/ERK1* is present in a
43 frequently mutated region of 16p11.2 linked to Autism Spectrum Disorder (ASD) and animal models of
44 Fragile X, Rett, and Angelmann Syndromes also exhibit changes in ERK/MAPK signaling activity (Kumar
45 et al., 2008; Pucilowska et al., 2015; Vorstman et al., 2006). These disorders are often associated with
46 intellectual disability, neurodevelopmental delay, ADHD, autism, and epilepsy. Clearly, aberrant
47 ERK/MAPK activity is an important molecular mediator of neurodevelopmental abnormalities, however,
48 therapeutic approaches for these conditions are lacking, due in part to a limited understanding of the
49 developmental stage- and cell-specific functions of ERK/MAPK signaling in the brain. Delineating the
50 precise consequences of altered ERK/MAPK activity on specific neuronal subtypes in the developing
51 forebrain may provide insight into the neuropathogenesis of multiple neurodevelopmental diseases.

52 Coordinated interactions between multiple cell types are necessary for normal brain function, but
53 deficits in select cellular subtypes often mediate specific neurodevelopmental phenotypes. Past work has
54 shown that ERK/MAPK signaling regulates the development of dorsal cortex-derived glutamatergic
55 cortical projection neurons (PNs) and glia (Aoidi et al., 2018; Ehrman et al., 2014; Ishii et al., 2013; Li et
56 al., 2012). Upstream regulators, such as *Syngap1*, are also crucial for the early development of cortical
57 glutamatergic neuron structure, excitability, and cognition (Clement et al., 2012; Ozkan et al., 2014). In
58 contrast, *NF1* mutations have been shown to impair aspects of spatial learning and memory via disruption
59 of GABAergic, but not glutamatergic, neuron function (Cui et al 2008). Abnormal GABAergic circuitry is
60 thought to be a key feature in the neuropathogenesis of various other neurodevelopmental disorders (Chao
61 et al., 2010; Cui et al., 2008; Paluszkiwicz et al., 2011; Zhang et al., 2010). GABAergic neuron-directed

62 *Syngap1* loss modulates GABAergic output but does not drive major abnormalities in mouse behavior or
63 seizure threshold (Berryer et al., 2016; Ozkan et al., 2014). Mutations in signaling components upstream of
64 *Ras* differentially modulate multiple downstream pathways and do not provide a clear delineation of
65 ERK/MAPK function (Anastasaki and Gutmann, 2014; Brown et al., 2012). Here, we have hyperactivated
66 MEK1 specifically in GABAergic cortical interneurons (CINs) to better understand the effects on inhibitory
67 circuit development.

68 In the mature cortex, locally connected parvalbumin- (PV) and somatostatin-expressing (SST)
69 CINs comprise the most populous and functionally diverse GABAergic subtypes (Kessaris et al., 2014).
70 Reduced PV-CIN number is often observed in mouse models of multiple neurodevelopmental diseases,
71 however, the mechanism of loss is poorly understood (Chao et al., 2010; Cui et al., 2008; Steullet et al.,
72 2017). PV- and SST-CINs are generated in spatiotemporal fashion primarily from the medial ganglionic
73 eminence (MGE) and migrate tangentially to the cortical plate (Gelman et al., 2009; Gelman and Marín,
74 2010; Lavdas et al., 1999; Marin and Rubenstein, 2001, 2003; Parnavelas, 2000; Tamamaki et al., 1997;
75 Wichterle et al., 1999; Wichterle et al., 2001; Wonders and Anderson, 2006). Tangential migration and
76 early GABAergic circuit development is regulated by BDNF/TRKB, GDNF/GFR α 1, HGF/MET, and
77 NRG/ERBB4 signaling, which activate multiple Receptor Tyrosine Kinase (RTK)-linked intracellular
78 kinase cascades, including ERK/MAPK (Bae et al., 2010; Fazzari et al., 2010; Flames et al., 2004;
79 Perrinjaquet et al., 2011; Pozas and Ibanez, 2005). While the transcriptional basis of GABAergic neuron
80 development has been well-studied (Lim et al., 2018; Mayer et al., 2018; Mi et al., 2018; Paul et al., 2017),
81 the kinase cascades that mediate GABAergic development in response to critical extracellular cues have
82 received less attention.

83 Here, we show that GABAergic neuron-specific expression of constitutively-active MEK1^{S217/221E}
84 (caMEK1) led to caspase-3 activation in a subset of embryonic GABAergic neurons. Even though caMEK1
85 is expressed in all CINs, we only observed a significant reduction in the number of mature PV-CINs, but
86 not SST-CINs. In contrast with past models exhibiting PV-CIN loss, we found a surprising increase in the
87 extent of perineuronal net (PNN) accumulation around these cells (Steullet et al., 2017). We observed an

88 increased risk of spontaneous epileptiform activity and mild seizure-like activity in a subset of mutant mice
89 that coincided with a reduction in inhibitory synapses on pyramidal neurons. Mutant mice exhibited normal
90 locomotor, anxiety-like, and social behaviors, but we discovered deficits in behavioral response inhibition
91 capacity, a process linked to ADHD-like phenotypes. Our findings indicate that GABAergic-specific
92 MEK1 hyperactivation is sufficient to drive widespread changes in cortical development relevant to
93 cognitive phenotypes observed in RASopathies. Together, these data define the precise functions of
94 ERK/MAPK signaling in CIN development and suggest preferential contributions of PV-CIN pathology to
95 ERK/MAPK-linked disorders.

96

97 **Results**

98 *Differential expression of ERK/MAPK components in CINs*

99 The ERK/MAPK cascade is a commonly utilized intracellular signaling pathway that is
100 dynamically activated during embryogenesis and in adulthood. In the embryonic ventricular zone, neural
101 progenitors typically show high levels of P-ERK1/2 relative to immature post-mitotic neurons (Pucilowska
102 et al., 2018; Stanco et al., 2014). In adult cortices, elevated P-ERK1/2 labeling is enriched in a
103 heterogeneous set of excitatory PNs, primarily in layer 2, and plays a critical role in long-range PN
104 development (Cancedda et al., 2003; Gauthier et al., 2007; Holter et al., 2019; Pham et al., 2004; Pucilowska
105 et al., 2012; Suzuki et al., 2004; Xing et al., 2016). The activation of ERK1/2 in CINs has not been well
106 characterized. We generated mice expressing *Slc32A1:Cre* and the Cre-dependent red fluorescent protein
107 (RFP) reporter, *Ai9* (Madisen et al., 2010; Vong et al., 2011) (Figure 1A-D). As expected, brain regions
108 abundant with GABA-expressing neurons robustly expressed *Ai9* (Figure 1A). Immunolabeling for
109 MAP2K1 (MEK1) revealed relatively lower expression in CINs in comparison to NEUN⁺/RFP⁺
110 presumptive PNs (Figure 1E-G). Layer II/III CINs also expressed low levels of MAPK1/ERK2 in
111 comparison to PNs (Figure 1H-J). In agreement with previous studies, high levels of P-ERK1/2 were
112 observed in a subset of PNs in cortical layer II/III (Cancedda et al., 2003; Pham et al., 2004; Suzuki et al.,
113 2004). However, examination of P-ERK1/2 immunolabeling in RFP⁺ CINs revealed qualitatively lower

114 levels of P-ERK1/2 in comparison to PNs (Figure 1K-M). In summary, CINs express relatively lower levels
115 of MEK1, ERK2, and P-ERK1/2 than excitatory neurons in the adult cortex, raising the possibility of
116 functionally distinct roles for this cascade between these two primary cortical neuron subtypes.

117

118 *GABAergic-autonomous caMEK1 expression decreases PV-CIN number*

119 Increased ERK/MAPK signaling is the most common result of RASopathy-linked mutations
120 (Tidyman and Rauen, 2016). We utilized a Cre-dependent, constitutively active *CAG-Loxp-Stop-Loxp-*
121 *Mek1*^{S217/221E} (*caMek1*) allele, which has been shown to hyperactivate MEK1/2-ERK1/2 signaling (Alessi
122 et al., 1994; Bueno et al., 2000; Cowley et al., 1994; Klesse et al., 1999; Krenz et al., 2008; Lajiness et al.,
123 2014; Li et al., 2012). We generated *caMek1, Slc32A1:Cre* mice to hyperactivate MEK1 in a CIN-specific
124 fashion during embryogenesis. Elevated MEK1 expression was clearly detectable in the E13.5 mantle zone
125 of the ganglionic eminences, presumptive embryonic CINs migrating into the cortex, and adult CINs in
126 primary somatosensory cortex (S1) (Figure S1A-H; J-O). *CaMek1, Slc32A1:Cre* mice were viable and
127 phenotypically normal, though mutants exhibited larger body mass than controls in adulthood (Figure S1I).

128 Surprisingly, assessment of fluorescently-labeled CINs in *caMek1, Slc32A1:Cre, Ai9* sensory
129 cortices revealed a significant reduction in total RFP⁺ cell density (Figure 2A-I). In the adult cortex,
130 approximately 40% of CINs express PV whereas 30% express SST, which serve as mostly non-overlapping
131 markers of two distinct populations of CINs (Kelsom and Lu, 2013; Kessaris et al., 2014; Rudy et al., 2011).
132 Strikingly, we observed a significant reduction in the proportion of PV⁺/RFP⁺ CINs, but not in the
133 proportion of SST⁺/RFP⁺ CINs (Figure 2K-Q). PV, but not SST, expressing CINs displayed a significant
134 increase in somal area compared to control neurons (Figure 2R-U, V). A reduced density of PV-CINs was
135 detected in a separate *caMek1, Dlx5/6:Cre* strain that also targets postmitotic CINs in the developing cortex
136 (Figure S2A-D) (Monory et al., 2006).

137 Recombination within the entire GABAergic system left open the possibility that indirect changes
138 in other neuroanatomical regions could alter global cortical activity and modulate PV-CIN number (Denaxa
139 et al., 2018). To restrict Cre expression to primarily MGE-derived CINs, we generated *caMek1, Nkx2.1:Cre,*

140 *Ai9* mice and assessed the proportion of PV⁺/RFP⁺ CINs. *CaMek1, Nkx2.1:Cre* mice exhibited generalized
141 growth delay in the second-third postnatal week and were not viable past the first postnatal month (n=8).
142 Nonetheless, consistent with our previous findings, P14 *caMek1, Nkx2.1:Cre, Ai9* mice displayed a
143 reduction in PV⁺/RFP⁺-CIN density (Figure S2E-L, M). In summary, our data indicate that the
144 establishment of PV-CIN number is cell-autonomously vulnerable to enhanced MEK1 signaling, while
145 SST-CIN number is not altered.

146

147 *Presumptive mutant PV-CINs in the embryonic subpallium undergo apoptosis*

148 Our analyses of RFP⁺ CINs in P3.5 *caMek1, Slc32A1:Cre* mice yielded a significant reduction in
149 CIN density, thus, we hypothesized that gain-of-function MEK1 signaling disrupted embryonic processes
150 necessary to establish CIN number. Indeed, examination of RFP⁺ CIN density in the E17.5 cortical plate
151 also revealed fewer CINs in *caMek1, Slc32A1:Cre* embryos (Figure S3A-D). We examined markers of
152 neuronal death during mid-neurogenesis in the *caMek1, Slc32A1:Cre, Ai9* subpallium. Immunolabeling for
153 the apoptotic marker cleaved caspase 3 (CC3) revealed colocalization of CC3 with some RFP⁺ neurons
154 within the mantle zone of the ganglionic eminences in E13.5 mutant, but not control, embryos (Figure 3A-
155 E, F). CC3⁺/RFP⁺ neurons also presented with condensed, pyknotic nuclei (Figure 3G-N). We also observed
156 CC3⁺/RFP⁺ cells with pyknotic nuclei in *caMek1, Nkx2.1:Cre, Ai9* mantle zone (Figure 3O-Q). No
157 apoptotic cells were observed in the mutant ganglionic eminence VZ or the cortical migratory streams.
158 Analysis of recombined GABAergic neuron density in the dorsal striatum did not reveal a significant
159 difference from controls, suggesting that the loss of PV-CINs is not due to altered CIN migratory trajectory.
160 Together, our results suggest reduced PV-CIN density in the postnatal cortex is due to the death of a subset
161 of migrating CINs in the ganglionic eminence.

162

163 *GABAergic-specific caMek1 promotes cortical hyperexcitability but does not significantly alter fast-spiking*
164 *CIN electrophysiological properties*

165 Nearly 40% of RASopathy individuals with mutations downstream of *RAS* experience seizures and
166 epilepsy (Digilio et al., 2011; Rauen et al., 2013; Yoon et al., 2007). Whether MEK1 hyperactivation in
167 GABAergic circuits mediates seizure activity in the RASopathies is unclear. We did not detect any signs
168 of overt generalized tonic-clonic seizures in mutant mice while housed in home cages. We conducted a
169 series of behavioral tests by first using the open field, then the elevated plus maze, and finally the social
170 approach assay. No difference in global locomotor activity, anxiety-like behavior, or sociability could be
171 detected with these tests (Figure S4). However, during the initial 60 sec of open field testing with 13 adult
172 *caMek1, Slc32A1:Cre* mutants, two mutant mice exhibited increased head twitching, aberrant locomotor
173 activity, and increased rearing (Supp. Video 1) and three mutant mice displayed periods of overt sudden
174 behavioral arrest and motionless staring (Supp Video 2). These behaviors were not observed in any of the
175 control mice utilized in this study. Consistent with these subtle impairments, subsequent re-analysis of the
176 first 10 sec of the open field task revealed a significant reduction in distance traveled in *caMek1,*
177 *Slc32A1:Cre* mutants, which was also observed in *caMek1, Dlx5/6:Cre* mutants.

178 We performed intracortical EEG recordings to directly assess cortical activity, which revealed
179 spontaneous epileptiform-like discharges in three of six *caMek1, Slc32A1:Cre* adult mice, but not control
180 mice (Figure 4A). These six mutants also exhibited a significantly reduced average threshold to seizure
181 induction in response to pentylenetetrazol (PTZ) administration when compared to controls (Figure 4B).
182 Seizures have been shown to increase the local expression of glial fibrillary acidic protein (GFAP) in
183 astrocytes (Steward et al., 1992; Stringer, 1996). 3 of 3 newly generated and untreated *caMek1 Slc32A1:Cre*
184 mice immunolabeled for GFAP exhibited clusters of GFAP-expressing astrocytes in the cortex consistent
185 with local reactive astrogliosis near hyperexcitable regions (Figure 4C-F). Overall, some of the seizure-
186 related phenotypes we observed were not completely penetrant, thus, these data indicate that MEK1
187 hyperactivation in CINs may be a potential risk factor for epilepsy in the RASopathies.

188 PV-CINs provide a powerful source of inhibition in the cortex, firing action potentials at
189 frequencies greater than 200Hz (Okaty et al., 2009). Fast-spiking (FS) physiology is due in part to the
190 unique expression of the fast-inactivating potassium channel Kv3.1, which begins in the second postnatal

191 week (Goldberg et al., 2011; Rosato-Siri et al., 2015; Rudy and McBain, 2001). To determine if hyperactive
192 MEK1 signaling was sufficient to alter basic physiological properties of FS CINs, we performed whole-
193 cell patch clamp recordings on *caMek1, Nkx2.1:Cre* mice at the end of the third postnatal week. Current
194 clamp recordings of fluorescently-labeled CINs revealed that both control and mutant neurons retained their
195 distinctive electrophysiological fast-spiking phenotype (Figure 4G, I) (Agmon & Connors, 2018; Anderson
196 et al., 2010; McCormick et al., 1985). No significant differences were observed in resting membrane
197 potential, adaptation index, rheobase, or action potential threshold, but a small increase in action potential
198 amplitude was observed (Figure 4I). We did also detect a significant increase in FS CIN input resistance
199 and a reduction in FI slope in *caMek1, Nkx2.1:Cre* mutant compared with *Nkx2.1:Cre* controls suggesting
200 that mutants may have a reduction in the responsiveness and/or firing output of inhibitory neurons (Figure
201 5H-I). Overall, these data indicate that canonical electrophysiological features of fast-spiking CIN
202 development were not altered by MEK1 hyperactivation. However, certain intrinsic properties exhibit
203 subtle differences in mutant mice that might contribute to circuit-wide hyperexcitability.

204

205 *Inhibitory synapse formation and perineuronal net accumulation are altered by MEK1 hyperactivity*

206 PV-expressing CINs preferentially innervate pyramidal cells, often forming synapses on the
207 perisomatic domain (Chattopadhyaya et al., 2004; Chattopadhyaya et al., 2007). We assessed whether
208 perisomatic VGAT-labeled synapses surrounding layer 2/3 PNs were diminished in adult *caMek1,*
209 *Slc32A1:Cre, Ai3* mice. We found the extent of VGAT-immunolabeling in the perisomatic space of
210 NEUN⁺/GFP⁺ PN soma was significantly reduced in mutant cortices when compared to controls (Fig. 5A-
211 F, M). Interestingly, the area of VGAT-labeling in the surrounding neuropil, typically innervated by SST-
212 CINs, was unchanged (Fig. S5A-F). These data show that PV-CIN inhibitory output is selectively
213 vulnerable to caMEK1 signaling while SST-CINs are less affected.

214 PV-CINs selectively accumulate an extracellular structure called the perineuronal net (PNN)
215 derived primarily from glial chondroitin sulfate proteoglycans (CSPGs). PNNs are essential to cortical
216 development, restricting plasticity during the closure of critical periods and protecting PV-CINs from

217 oxidative stress associated with a high frequency firing rate (Cabungcal et al., 2013; Hensch, 2005b).
218 Reductions in PNN formation have been noted in multiple models of neurodevelopmental disorders that
219 exhibit loss of PV-CINs (Bitanirwe and Woo, 2014; Cabungcal et al., 2013; Krencik et al., 2015; Krishnan
220 et al., 2015; Steullet et al., 2017). We utilized WFA-labeling to test whether PNN formation was reduced
221 in adult *caMek1*, *Slc32A1:Cre*, *Ai3* mice (Figure 5H-M). Surprisingly, we found that surviving PV-CINs
222 were WFA⁺ in mutants (Figure 5G-L). PNNs were also not detected on *Ai3*-expressing neurons that lacked
223 PV-expression. Consistent with the larger somal size of mutant PV-CINs, the cross-sectional area of WFA-
224 labeled profiles was also significantly increased (Figure 5G-L, N). Analysis of the quantitative level of
225 WFA-labeling in mutant PV-CINs revealed a robust increase in PNN accumulation as compared to controls
226 (Figure 5G-L, O). Mutant WFA-labeled CINs exhibited normal expression of 8-oxo-2'-deoxyguanosine (8-
227 oxo-dg), a marker of DNA oxidation often altered in neurons with reduced PNNs (Figure S5 F-I) (Steullet
228 et al., 2017). Collectively, MEK1 hyperactivation clearly increases PNN accumulation, but does not trigger
229 ectopic PNN formation on GABAergic neurons lacking PV.

230

231 *caMek1*, *Slc32A1:Cre* mice display delayed acquisition of FMI performance

232 Attention deficit hyperactivity disorder (ADHD) is associated with a significant proportion of
233 RASopathy cases (Adviento et al., 2014; Garg et al., 2013; Green et al., 2017; Pierpont et al., 2018; Walsh
234 et al., 2013). Altered prefrontal cortex (PFC) function has been implicated in ADHD (Gabay et al., 2018),
235 and has been shown to contribute to cognitive deficits in a mouse model of Fragile X Syndrome (Krueger
236 et al., 2011). Few studies have examined GABAergic contributions to PFC function in the context of
237 RASopathies. As in sensory cortex, we noted a reduction in *Ai9*-expressing CINs in the PFC of mutant mice
238 (Figure 6A-B, D-E). Interestingly, we found that PNs in the PFC exhibit reduced P-ERK1/2 expression in
239 *caMek1*, *Slc32A1:Cre* mice (Figure 6A-F). These data indicate that MEK1 hyperactivation in developing
240 CINs is sufficient to drive molecular abnormalities within specific cortical regions important for cognition.

241 Individuals with ADHD often exhibit structural changes in the PFC, which appear to be involved
242 in the inhibition of reinforced responses (Seidman et al., 2006). To examine response inhibition directly,

243 we utilized a fixed minimum interval (FMI) test, a timing-based task that requires animals to withhold a
244 response for a fixed period. This paradigm is perhaps more favorable than the five-choice serial reaction
245 time task (5-CSRTT) and differential reinforcement of low rates task (DRL), because its self-paced design
246 dissociates response inhibition capacity from motivational aspects of behavior (Bizarro et al., 2003;
247 Doughty and Richards, 2002; Hill et al., 2012; Watterson et al., 2015). Here, adult control and *caMek1*,
248 *Slc32A1:Cre* mice were trained to initiate trials via a nose-poke which resulted in the presentation of
249 sweetened condensed milk in the reward receptacle. Mice were then placed on an FMI schedule, where a
250 time delay between the initiating nose-poke and the availability of reinforcement in the reward receptacle
251 was implemented (Figure 8G). Reward was delivered only if the time between the initiating nose-poke and
252 attempt to obtain reward (inter-response time, or IRT) exceeded a pre-determined withholding period. If
253 mice prematurely accessed the reward receptacle, no reward was delivered.

254 Following initial training on a FMI with a very short (0.5s) response-withholding period, we
255 measured mouse performance when the withholding period was extended to 2s, 4s, and finally, 8s. We
256 observed a main effect of FMI schedule irrespective of genotype, such that IRTs increased as the FMI
257 withholding period increased ($F(2, 62) = 535.12, p < 0.01$). Importantly, mutants showed clear evidence
258 of impaired acquisition of the FMI task. We found a main effect of genotype on the mean median IRT
259 during the first 5 days of each FMI schedule (acquisition period), in which mutant mice had relatively lower
260 IRTs compared to control mice ($F(1, 62) = 18.73, p < 0.01$) (Figure 6H). In further support of reduced
261 response inhibition capacity, mutant mice exhibited increased variability in their IRTs as measured by the
262 coefficient of quartile variation (CQV) during acquisition ($F(1, 62) = 31.73, p < 0.01$) and asymptotic
263 performance (defined as the last five days of the FMI) ($F(2, 62) = 5.055, p < 0.001$) across all schedules
264 (Figure 6I). Median IRTs during the asymptotic phase in mutants and controls were not statistically
265 different in any schedule (Figure 6H inset). Thus, these data suggest that mutant mice are capable of
266 learning to inhibit reinforced responses for up to 4 s but show a significant delay in acquiring this capability.

267 Due to *Slc32A1:Cre*-mediated recombination within subcortical circuitry, it is possible that altered
268 reward pathway activity influenced FMI performance. The latency to initiate (LTI) a trial provides a

269 measure of motivation; for example, rats administered amphetamine show a reduction in LTI in a related
270 task (Rojas-Leguizamón et al., 2018). However, we noted that mutants did not differ from controls in the
271 median LTI at 2s and 4s, indicating that motivation to obtain rewards was not significantly altered between
272 conditions (Tukey's b post-hoc test - 2s: $t(21) = 1.39$, $p=0.18$; 4s: $t(21) = -0.29$, $p=0.77$) (Figure 6J). We
273 found that during the 8s FMI, mutant mice exhibited a statistically significant increase in LTI ($t(20) = 2.43$,
274 $p < 0.05$). This apparent loss of motivation is likely due to the fact that the mean median asymptotic IRT
275 did not reach the 8s criterion even after 32 days of testing (control: $8.45s \pm 1.04$; mutant: $7.26s \pm 1.09$) and
276 is also consistent with the statistically significant reduction in mean obtained reinforcers at the 8s FMI
277 (Figure 6K). Collectively, our data indicate that altered GABAergic circuitry regulates acquisition of
278 response inhibition capacity in mice and may contribute to ADHD phenotypes associated with the
279 RASopathies.

280

281 Discussion

282 Here, we show that GABAergic neuron-autonomous MEK1 hyperactivation causes the death of a
283 subset of immature GABAergic neurons in the embryonic subpallium and is associated with a selective
284 reduction in PV-CIN density, but not SST-CINs, in adulthood. We observed a significant reduction in
285 perisomatic GABAergic synapses on layer 2/3 PNs and forebrain hyperexcitability, but a surprising
286 increase in the extent of PNN accumulation in mutant PV-CINs. While mutants displayed relatively normal
287 performance in assays of locomotion, sociability, and anxiety, we found notable defects in acquisition of
288 behavioral response inhibition capacity, which has been linked to ADHD. These data suggest that
289 GABAergic neuron-autonomous MEK1 hyperactivation selectively regulates embryonic PV-CIN survival
290 and is an important contributor to seizure risk and cognitive deficits in the RASopathies.

291 While expression of ERK/MAPK pathway components is widespread, our findings reinforce the
292 notion that expression levels are variable, and activation of this cascade is highly cell-type dependent. Cell-
293 specific transcriptomic experiments have reported that RNA levels of *Mapk1/Erk2* and *Map2k1/Mek1*, but
294 not *Mapk3/Erk1* or *Map2k2/Mek2*, are lower in CINs relative to PNs (Mardinly et al., 2016). We have

295 extended these findings to show that protein levels of MAPK1/ERK2 and MAP2K1/MEK1 are typically
296 lower in CINs than in surrounding PNs. Reduced expression of pan-ERK/MAPK components may
297 contribute to the relatively low levels of phosphorylated ERK1/2 in CINs. Past work has shown that the
298 experience-dependent transcriptional response in V1 PV-CINs is significantly smaller relative to PNs
299 (Hrvatin et al., 2018). A more stringent degree of ERK/MAPK recruitment in CINs might contribute to
300 reduced activity-dependent transcription. Further analysis of activity-dependent responses in ERK/MAPK-
301 mutant mice may assist in defining how CIN-specific functional properties are encoded (Tyssowski et al.,
302 2018).

303 Defects in GABAergic circuitry have been implicated in the pathogenesis of Rett, Fragile X,
304 schizophrenia and many other neurodevelopmental diseases (Chao et al., 2010; Cui et al., 2008; Steullet et
305 al., 2017). Reduced PV-CIN number is often observed, however, the mechanism of loss is poorly
306 understood. We show that MEK1 hyperactivation drives the GABAergic-neuron autonomous activation of
307 caspase-3 and death of a subset of immature neurons in the embryonic ganglionic eminences. The selective
308 reduction in PV-CIN density in the postnatal cortex suggests these early dying neurons were committed to
309 the PV lineage. The death of this specific subset of GABAergic neurons occurs much earlier than the typical
310 period of programmed cell death for CINs (Denaxa et al., 2018; Southwell et al., 2012) . Notably, *caMek1*
311 expression in cortical excitatory neurons is not associated with significant neuronal loss during development
312 (Nateri et al., 2007; Xing et al., 2016). Though ERK/MAPK typically acts as a promoter of cell survival,
313 apoptotic death by sustained ERK/MAPK activity has been described in certain contexts (Cagnol and
314 Chambard, 2010; Martin and Pognonec, 2010). It will be important to evaluate whether treatment with
315 pharmacological MEK1/2 inhibitors or antioxidants during embryogenesis is capable of sustained
316 restoration of CIN number in *caMek1*, *Slc32A1:Cre* mice. PV-CIN sensitivity to MEK1 hyperactivation
317 may not only be an important factor in RASopathy neuropathology, but could be a relevant mechanism in
318 other conditions that involve indirect activation of ERK/MAPK signaling during embryogenesis, such as
319 schizophrenia, Fragile X Syndrome, or prenatal stress (Fowke et al., 2018).

320 Recent scRNAseq analyses suggest the mature transcriptional signature of cardinal CIN subtypes
321 is not fully specified until CINs migrate into the cortex (Mayer et al., 2018; Paul et al., 2017; Sandberg et
322 al., 2018). MEF2C, a known substrate of ERK1/2 and p38 signaling, was identified as a transcription factor
323 expressed early in the presumptive PV lineage, the deletion of which also leads to the selective reduction
324 of PV-CINs (Mayer et al., 2018). Thus, regulation of MEF2C could mediate early effects of caMEK1
325 signaling on GABAergic neuron development. While further research is necessary, the selective
326 vulnerability of presumptive PV-CINs to hyperactive MEK1 signaling may not be dependent upon a
327 specific downstream transcriptional target. Compared to transcriptional networks, less is known regarding
328 the function of many post-translational modifications during CIN specification. Our data hint at selective
329 roles for kinase signaling networks at an early stage of CIN lineage differentiation.

330 Despite the effect of caMEK1 on early GABAergic neuron survival, the physiological maturation
331 of mature *caMek1*-expressing PV-CINs was not significantly impeded. Surviving PV-CINs retained a
332 characteristic fast-spiking signature with only minor differences in intrinsic electrophysiological
333 parameters. We noted a modest, but statistically significant decrease in perisomatic inhibitory synapse
334 number on cortical PNs in mutant mice. As might be expected, a subset of mutant animals exhibited
335 forebrain hyperexcitability and sudden behavioral arrest similar to that reported in animal models of mild
336 seizures. Overexpression of a similar *caMek1* mutation with *CamKII:Cre* has also been shown to cause
337 seizure-like activity (Nateri et al., 2007). Overall, our findings indicate that MEK1 hyperactivation in
338 GABAergic neurons could increase the risk of epilepsy seen in RASopathies.

339 The PNN is a critically important structure involved in the maturation of cortical circuitry with an
340 important role in protecting PV-CINs from oxidative stress and limiting synaptic plasticity (Cabungcal et
341 al., 2013; Hensch, 2005a; Hensch, 2005b; Morishita et al., 2015). Mouse models of schizophrenia, Fragile
342 X, and ASDs often exhibit reduced PV-CIN number and typically display a reduction in PNN formation
343 (Steullet et al., 2017). In contrast to these disorders, PNNs appear to respond differently to RASopathy
344 mutations. PV-CINs accumulate extracellular PNNs derived primarily from astrocyte-produced CSPGs
345 (Galtrey and Fawcett, 2007; Sorg et al., 2016). RASopathic astrocytes upregulate secreted ECM-associated

346 CSPGs and promote an increase in the extent of PNN accumulation around PV-CINs (Krencik et al., 2015).
347 Our data is the first to indicate a PV-CIN autonomous role for enhanced PNN accumulation in response to
348 MEK1 hyperactivation. It is thought that increased PNN accumulation on PV-CINs limits the plasticity of
349 cortical regions (Pizzorusso et al., 2002). Modification of PNN levels may serve as a useful therapeutic
350 strategy for the impaired cognitive function and intellectual disability frequently reported in RASopathy
351 individuals (Tidyman and Rauen, 2016).

352 In addition to intellectual disability, ADHD is frequently diagnosed in Noonan Syndrome and NF1,
353 two common RASopathies (Johnson et al., 2019; Miguel et al., 2015; Pierpont et al., 2015). Abnormal PFC
354 function has been linked to ADHD (Seidman et al., 2006). Interestingly, we detected significantly reduced
355 P-ERK1/2 levels in PFC PNs of mutant mice, suggesting that RASopathic CINs may alter the global
356 development and function of this brain region. GABAergic signaling is known to be necessary for cortical
357 circuit maturation (Cancedda et al., 2007). We further examined ADHD-related behavioral phenotypes in
358 *caMek1*, *Slc32A1:Cre* mice by assessing behavioral response inhibition capacity with a fixed-minimum
359 interval (FMI) based task (Rojas-Leguizamón et al., 2018; Watterson et al., 2015). We detected significant
360 deficits in the acquisition of response inhibition dependent behaviors in mutant mice relative to controls. It
361 is plausible that FMI defects in *caMEK1* mutants is due to the reduced plasticity of PFC GABAergic
362 circuitry in response to heightened levels of PNN or GABAergic-dependent changes in PN development.
363 These data show that GABAergic-directed MEK1 hyperactivation is sufficient to drive deficits in
364 behavioral response inhibition possibly associated with ADHD.

365 Mutations in ‘upstream’ RASopathy genes modulate a much broader set of downstream cascades
366 when compared to mutations in *Raf* or *Mek1/2*. *Nf1*, *Ptpn11/Shp2*, and *Syngap1* mutations result in a
367 complex constellation of cellular changes, some of which depend upon ERK/MAPK modulation, whereas
368 others involve different signaling cascades (Anastasaki and Gutmann, 2014; Brown et al., 2012). In
369 combination with the findings of (Angara et al., 2019, co-submitted), it is clear that PV-CIN development
370 is particularly sensitive to convergent signaling via NF1 and ERK/MAPK. Additional studies of human
371 samples will be necessary to determine whether defective GABAergic circuits are a component of

372 RASopathy pathogenesis. Collectively, our research suggests that hyperactivation of MEK1 in GABAergic
373 neurons represents an important candidate mechanism for epilepsy and cognitive defects in RASopathic
374 individuals.

375 **Acknowledgements**

376 We would like to thank Johan Martinez, Sam Lusk, Julia Pringle, Anna Kreuger, Sarah Sparks, Katie
377 Riordan, Danielle Gonzalez, Elise Bouchal, and Kimberly Holter for their technical contributions to this
378 work. This research is supported by National Institute of Health grants R00NS076661 and R01NS097537
379 awarded to JMN, R01NS087031 awarded to TRA, and R01NS031768 to WDS.

380

381 **Author Contributions**

382 Conceptualization, J.M.N, W.D.S, M.C.H, C.W.D, F.S., T.R.A.; Methodology, J.M.N, W.D.S, M.C.H,
383 C.W.D, F.S., T.R.A., S.M., D.M.T.; Investigation, J.M.N, W.D.S, M.C.H, L.T.H., K.N., G.R.B., S.S.,
384 N.R.F., K.P.R., T.A.G., G.L., M.F.O., C.W.D, F.S., T.R.A., S.M., D.M.T.; Writing – Original Draft,
385 M.C.H., J.M.N., C.W.D., T.A.G., F.S., T.R.A., S.M., M.F.O., L.T.H., K.N.; Writing –
386 Review & Editing, M.C.H., J.M.N., G.R.B., S.S., N.R.F., K.P.R., D.M.T. ; Funding Acquisition, J.M.N
387 and W.D.S.; Resources, J.M.N, T.R.A., W.D.S., D.M.T., M.F.O., F.S.; Supervision, J.M.N., W.D.S.,
388 D.M.T., T.R.A., F.S.

389

390 **Declaration of Interest**

391 The authors declare no competing interests.

392 **Figure Titles and Legends**

393 *Figure 1. Cortical CINs exhibit low levels of ERK/MAPK expression and activity.*

394 **(A-D)** Representative confocal images of *Slc32A1:Cre, Ai9* sensorimotor cortex. Note the robust expression
395 of RFP in brain regions with high densities of GABAergic neurons. (Scale bar = 100 μ m) **(E-M)**
396 Immunolabeling for MEK1 (E-G) and ERK2 (H-J) showed comparatively low expression in inhibitory
397 CINs (yellow outlines) when compared to NEUN⁺/*Ai9*⁻ excitatory neurons (arrowheads) in layer II (n=3).
398 Relatively lower expression of P-ERK1/2 was also detected in inhibitory CINs when compared to excitatory
399 neurons (n=3). (Scale bar = 10 μ m).

400

401 *Figure 2. MEK1 hyperactivation leads to a selective reduction in PV-expressing CINs in the postnatal*
402 *cortex.*

403 **(A-H)** *caMek1, Slc32A1:Cre, Ai9* mutant P3.5 (A-D) and P60 (E-H) primary somatosensory cortices exhibit
404 reduced numbers of *Ai9*-expressing CINs in comparison to *Slc32A1:Cre, Ai9* controls (quantification in **I**,
405 n=3, mean \pm SEM, * = p < 0.05). (Scale bar = 100 μ m) **(J-Q)** We quantified the proportion of fluorescently
406 co-labeled PV/RFP or SST/RFP co-expressing CINs in the sensory cortex (J). Confocal micrographs of
407 RFP-expressing CINs at P60 demonstrates that the proportion of PV⁺/RFP⁺ CINs, but not SST⁺/RFP⁺ CINs,
408 was significantly decreased in mutants (N-P) in comparison to controls (K-M) (quantification in **Q**: n=3,
409 mean \pm SEM, * = p < 0.05). (Scale bar = 100 μ m) **(R-V)** Mutant PV-CINs (T-U, green arrowheads in T)
410 display increased soma size in comparison to control PV-CINs (R-S) (quantification in **V**, n = 21 control
411 neurons, 42 mutant neurons, mean \pm SEM, * = p < 0.001). PV/RFP⁺ CINs displayed no qualitative change
412 in soma size (blue arrowheads). (Scale bar = 25 μ m).

413

414 *Figure 3. A subset of immature GABAergic neurons undergo cell death during mid-embryogenesis.*

415 **(A)** E13.5 coronal section of RFP-labeled CINs in the mantle zones of the *Slc32A1:Cre* subpallium during
416 mid-embryogenesis. **(B-F)** Immunolabeling for cleaved caspase 3 (CC3) showed a significant increase in
417 the number of apoptotic profiles in *caMek1, Slc32A1:Cre* mutants (D-E) as compared to controls (B-C)

418 (quantification in **F**; $n=3$, mean \pm SEM, * = $p < 0.05$). (Scale bar = 100 μm) (**G-Q**) Representative confocal
419 z-stacks of CC3 labeled cells from *caMek1*, *Slc32A1:Cre* embryos (G-N, Scale bar = 2 μm) and *caMek1*,
420 *Nkx2.1:Cre* embryos (O-Q) show clear colocalization with RFP and a condensed, pyknotic nuclear
421 morphology. See also Figure S4.

422

423 *Figure 4. caMek1 Slc32A1:Cre* CINs maintain typical fast-spiking properties, but a subset of mice exhibit
424 seizure-like phenotypes.

425 (**A**) Representative traces from forebrain-penetrating EEG revealed epochs of synchronous firing in 3 of 6
426 *caMek1 Slc32A1:Cre*, but not control mice. (**B**) Tail vein PTZ injections revealed a significant reduction in
427 mean dose to seizure onset of PTZ ($n = 6$, mean \pm SEM, * = $p < 0.001$). (**C-F**) *caMek1 Slc32A1:Cre* cortices
428 display aberrant clusters of GFAP-labeled astrocytes (**E**, arrowheads, insets in **F**) that were not observed in
429 controls (C-D) ($n=3$). (Scale bar = 100 μm) (**G**) Representative current clamp recordings of FS CINs in P21
430 *Nkx2.1:Cre Ai9* and *caMek1 Nkx2.1:Cre Ai9* mutant cortices. (**H**) Mutant CINs had a significantly reduced
431 FI slope in comparison to controls (mean \pm SEM, $p < 0.05$). (**K**) Summary table of FS CIN intrinsic
432 properties. See also Figure S5.

433

434 *Figure 5. Reduced perisomatic synapse labeling in mutant cortices coincide with a substantial increase in*
435 *PNN formation on PV-CINs.*

436 (**A-F**) Representative high-resolution confocal Airyscan images of triple immunolabeled cortical sections
437 for Ai3/EYFP, VGAT, and NEUN. Excitatory neuron perisomatic domains were outlined and
438 quantification of VGAT-labeled pixels revealed that mutants (D-F) have a significant reduction in the
439 amount of perisomatic VGAT-labeling (Scale bar = 3 μm) in comparison to controls (A-C)
440 (quantification in **M**; $n = 48$ control, 53 mutant neurons; mean \pm SEM, * = $p < 0.05$). (**G-L**) P60
441 representative coronal sections of *Slc32A1:Cre Ai3* (G-I) and *caMek1 Slc32A1:Cre Ai3* (J-L) cortices
442 immunolabeled for GFP, WFA, and PV. The WFA channel was imaged using the same acquisition
443 settings for all samples. A significant increase in WFA-labeled area per neuron was detected in mutant

444 cortices when compared to controls (quantification in **N**; n = 63 control, 54 mutant neurons, mean \pm SEM,
445 * = p < 0.001). Analysis of WFA-labeling intensity yielded a significant increase in integrated density in
446 mutant CINs (quantification in **O**; n = 63 control, 54 mutant neurons, mean \pm SEM, * = p < 0.001). (Scale
447 bar = 100 μ m).

448

449 *Figure 6. caMEK1 Slc32A1:Cre mice exhibit reduced behavioral response inhibition capacity.*

450 **(A-F)**. P-ERK1/2 labeling in PFC PNs is significantly reduced in mutants as compared to controls. Note
451 the decrease in RFP⁺ CINs in the mutant PFC (E) relative to control (B) (n=3). (Scale bar = 100 μ m)

452 **(G)** Schematic of the Fixed-minimum Interval (FMI) task. **(H)** Mutant mice had a significant reduction in

453 mean median IRT during FMI acquisition in 2s and 4s schedules (n=12, mean \pm SEM, * = p < 0.05). **(I)**

454 Mutant mean CQV of IRTs during both acquisition and asymptotic phases was significantly increased in

455 2s, 4s, and 8s FMI schedules (mean \pm SEM, * = p < 0.05). **(J)** Median acquisition and asymptotic LTI

456 was significantly increased in the FMI 8s, but not in the 2s and 4s schedules (mean \pm SEM, * = p < 0.05).

457 **(K)** Mutant mice had a reduction in mean acquisition ORs at 4s and a significant reduction in both mean

458 acquisition and asymptotic ORs during the 8s FMI (mean \pm SEM, * = p < 0.05).

459 **Methods**

460 *Mice*

461 All transgenic mice were handled and housed in accordance with the guidelines of the Institutional
462 Animal Care and Use Committee at Arizona State University, the University of Arizona, and Barrow
463 Neurological Institute. Mice were kept on a daily 12-hour light-dark cycle and were fed *ad libitum*.
464 *Slc32A1:Cre^{+/+}*, *Dlx5/6:Cre^{+/-}*, or *Nkx2.1:Cre^{+/-}* mice were crossed with *CAG-lox-STOP-lox-Mek1^{S217/221E+/-}*
465 (caMEK1) mice to generate mutants expressing *caMek1* in Cre-expressing cell types (Table S1). *CaMek1*
466 mice were kindly provided by Dr. Maïke Krenz and Dr. Jeffrey Robbins. Littermates expressing Cre-
467 Recombinase were utilized as controls for most experiments, unless otherwise indicated. Cre-dependent
468 tdTomato (*Ai9*) or eYFP (*Ai3*) strains were used to endogenously label Cre-expressing cells for
469 visualization purposes. Genomic DNA was extracted from tail or toe samples for standard genotyping by
470 PCR using the following primer combinations: (listed 5'-3'): Cre – TTCGCAAGAACCTGATGGAC and
471 CATTGCTGTCACTTGGTCGT to amplify a 266 bp fragment; *caMek1^{S217/221E}* -
472 GTACCAGCTCGGCGGAGACCAA and TTGATCACAGCAATGCTAACTTTC amplify a 600 bp
473 fragment; *Ai3/Ai9* – AAGGGAGCTGCAGTGGAGTA, CCGAAAATCTGTGGGAAGTC,
474 ACATGGTCCTGCTGGAGTTC, and GGCATTAAAGCAGCGTATCC amplify a 297 bp wt *Rosa26*
475 segment and a 212 bp *Ai3/Ai9* allele.

476

477 *Tissue Preparation and Immunostaining*

478 Mice of the appropriate postnatal age were anesthetized and transcardially perfused with PBS
479 followed by cold 4% PFA in PBS. Brains were dissected, post-fixed at 4°C, and sectioned with a vibratome
480 or cryopreserved with 30% sucrose and sectioned with a cryostat. Free-floating sections were incubated in
481 primary antibody solution consisting of 1X PBS with 0.05 - 0.2% Triton and 5% Normal Donkey Serum
482 (NDS). Sections were then incubated in species-specific, fluorescently-conjugated secondary antibodies in
483 blocking solution overnight. For embryonic sections, timed-bred embryos were collected at the appropriate
484 embryonic age, immersion fixed in cold 4% PFA in 1X PBS and cryopreserved in serial sucrose

485 concentrations (15%, 25% in 1X PBS) until fully infiltrated. Embryonic brain sections were cryosectioned
486 and directly mounted onto Fisher Superfrost Plus slides. Sections were gently rinsed in 1X PBS 0.05%
487 Triton, incubated in blocking solution (1X PBST 0.05% Triton and 5% NDS) and incubated overnight in
488 primary antibody prepared in blocking solution. The primary antibodies used in these experiments were:
489 goat anti-parvalbumin (Swant, 1:1000), rabbit anti-somatostatin (Peninsula, 1:1000), biotin-conjugated
490 WFA (Vector, 60ug/mL), chicken anti-GFP (Aves, 1:1000), chicken anti-RFP (Rockland, 1:1000), rabbit
491 anti-P-ERK (Cell Signaling, 1:1000), rabbit anti-MEK1 (Abcam, 1:1000), rabbit anti-ERK2 (Abcam,
492 1:1000), rabbit anti P-ERK1/2 (Cell Signaling, 1:1000), mouse anti-NEUN (Millipore 1:1000), rabbit anti-
493 cleaved caspase 3 (Cell Signaling, 1:1000), rabbit anti-GFAP (Abcam 1:1000), rabbit anti-VGAT (Synaptic
494 Systems, 1:1000), and mouse anti-8-oxo-DG (R&D Systems, 1:1000) (Table S2). Tissue was then washed
495 in 1X PBS 0.05% Triton and incubated in fluorescently conjugated secondary antibody solution before
496 rinsing and cover-slipping for microscopic analysis. Alexa-Fluor 488, 568, and 647 conjugated anti-rabbit,
497 anti-goat, and anti-chicken antibodies were diluted to 1:1000 in 1X PBS 0.05 – 0.2% Triton and 5% NDS.
498 Streptavidin-conjugated fluorophores were used to visualize WFA labeling. Representative images were
499 collected on a Zeiss (LSM710 & LSM800) laser scanning confocal microscope and optimized for
500 brightness and contrast in Adobe Photoshop.

501

502 *Image Analysis*

503 Images of at least three anatomically matched sections that include a brain region of interest were
504 quantified for labeled cell density by observers blind to genotype. For estimating labeled cell density in the
505 cortex, a column spanning all cortical layers was defined, the cross-sectional area measured, and the number
506 of labeled cells was assessed. The proportion of cells co-labeled with Cre-dependent fluorescent reporters
507 was also determined for select experiments. Quantification of cellular labeling was averaged across all
508 images collected from an individual mouse. At least three mice were collected for each genotype and results
509 were analyzed using Student's t-tests unless indicated otherwise.

510 We quantified the extent of inhibitory synapse labeling in the perisomal domain of excitatory
511 neurons from confocal images of VGAT/NEUN/GFP co-labeled sections. Confocal images were collected
512 using optimal Airyscan settings for a 63x 1.4 NA objective on a Zeiss LSM800 with the same acquisition
513 parameters, laser power, gain, and offset for VGAT detection. NEUN⁺/GFP⁻ neurons in S1 layer 2/3 with a
514 pyramidal morphology and residing 5-10µm from the tissue section surface were randomly selected by a
515 blinded observer. NEUN⁺ soma were outlined in Photoshop and a ring 1.8µm in thickness was then
516 established to specify the perisomatic space. VGAT-immunolabeling from perisomatic regions of interest
517 were imported into ImageJ where a moment-preserving autothreshold algorithm, “Moments”, was utilized
518 to define the total area of perisomatic VGAT-labeling in an unbiased manner. The perisomal VGAT-labeled
519 area was then normalized to the total perisomatic area for that neuron. A total of 48 control and 53 mutant
520 neurons from three different mice were analyzed. A similar approach was utilized to quantify VGAT
521 labeling in areas enriched in dendrites by analyzing randomly selected regions of the layer 2/3 neuropil that
522 did not incorporate any NEUN-labeled soma.

523

524 *EEG Recordings and Seizure Threshold Assessment*

525 Adult *caMek1*, *Slc32A1:Cre* mutant and *Slc32A1:Cre* control mice were assessed for epileptiform
526 activity with bilateral 175µm tungsten wires implanted in the forebrain. After recovery from electrode
527 implantation, mice were connected to suspended EEG leads, housed individually, and monitored daily in
528 home cages for seizure-like activity using a 128 channel Natus Medical EEG machine. EEG recordings
529 were examined for synchronous firing between hemispheres and representative epileptiform traces were
530 acquired. Following intracranial recording, mice were injected with the seizure inducing compound,
531 Pentylenetetrazol (PTZ; Sigma P6500). Mice were gently restrained and the tail vein was intravenously
532 injected with 0.34ml/min of 5mg/mL PTZ in 0.9% saline 10USP heparin by automated pump. Initial onset
533 of seizure was defined as the first sign of involuntary movement by an observer blinded to genotype. Time
534 to seizure was recorded and PTZ µg/g of body weight was calculated.

535

536 *Slice electrophysiology*

537 *caMek1^{+/-}*, *Nkx2.1:Cre^{+/-}*, *Ai9^{+/-}* mutant and *Nkx2.1:Cre^{+/-}*, *Ai9^{+/-}*-control mice were sacrificed
538 between postnatal day 21 to 24 and used for the in vitro slice electrophysiology. Brain slicing was performed
539 as reported previously (Nichols et al., 2018). In brief, mice were deeply anesthetized by isoflurane
540 inhalation before decapitation. Brains were quickly removed and the coronal slices (350 μ M) of the
541 somatosensory cortex were produced on a vibratome (VT 1200; Leica, Nussloch, Germany) in fully
542 oxygenated (95% O₂, 5% CO₂), ice-cold artificial cerebral spinal fluid (aCSF) containing (in mM): 126
543 NaCl, 26 NaHCO₃, 2.5 KCl, 10 glucose, 1.25 Na₂H₂PO₄·H₂O, 1 MgSO₄·7H₂O, 2 CaCl₂·H₂O, pH 7.4. The
544 slices were incubated in the same aCSF at 32°C for 30min before being allowed to recover at room
545 temperature for an additional 30 min before patch clamp recordings were started.

546 After recovery, slices were transferred into recording chamber and perfused continuously with
547 aCSF of 32°C at a rate of 1-2 ml/min. Then whole-cell patch clamp recordings were performed on
548 tdTomato-positive fast-spiking (FS) interneurons in the somatosensory cortex layer V/VI (L5/6) by using
549 an Axon 700B amplifier. The FS neurons were identified by lack of an emerging apical dendrite and their
550 intrinsic firing response to current injection (Agmon & Connors, 2018; Anderson et al., 2010; McCormick
551 et al., 1985). Clampex 10.6 (Molecular Devices) was used to collect data and pipettes (2-5 M Ω) were pulled
552 from borosilicate glass (BF150-110-10, Sutter Instruments) by using sutter puller (Model P-1000, Sutter
553 Instruments), filled with an internal solution that contains (in mM): 135 K-Gluconate, 4 KCl, 2 NaCl, 10
554 HEPES, 4 EGTA, 4 Mg ATP and 0.3 Na Tris. The stability of the recordings was monitored during the
555 experiments, and only the recordings with the series resistances (R_s) less than both 25 M Ω and 20% of the
556 membrane resistances were chosen for analysis. For the input resistance calculation, the steady plateau of
557 the voltage responding to the current input of -50 pA step with 1 s duration was used and intrinsic
558 parameters were measured as previously reported (Nichols et al., 2018). Adaptation index was calculated
559 as the ratio of the 1st interspike interval over the last (i.e. F_{1st ISI}/F_{last ISI}). The frequency (F) – current (I)
560 slope was calculated as the number of induced action potentials (APs) divided by the current step (number

561 of APs at 150pA-number of APs at 100pA)/(150pA-100pA). Unpaired Student's t-test and two-way
562 ANOVA with Bonferroni post hoc tests were used for statistical analysis.

563

564 *Behavioral Testing*

565 *Open Field Testing*

566 The open field test was used to test voluntary locomotor capabilities and anxiety-like behavior. The
567 apparatus consisted of a 40x40cm arena enclosed by 30cm high opaque walls. A single 60W bulb was
568 positioned to brightly illuminate the center of the chamber with dim lighting near the walls. Mice were
569 placed into the apparatus and recorded for a total of 10 minutes. Video data were analyzed for total distance
570 traveled and time spent in the center quadrant.

571

572 *Elevated Plus Maze*

573 The elevated plus maze was constructed from black polycarbonate, elevated 81cm off the ground,
574 and oriented in a plus formation with two 12x55cm open arms and two 12x55cm closed arms extending
575 from an open 12x12cm center square. Closed arm walls were 40cm high extending from the base of the
576 arm at the center square. The apparatus was lit with a 60W bulb with light concentrated on the center square.
577 At the beginning of the trial, mice were placed in the center square, facing the south open arm, and recorded
578 while freely exploring for 5 minutes.

579

580 *Social Approach Assay*

581 The social approach apparatus was made of transparent plexiglass and contained three 20x30x30cm
582 chambers (total dimensions 60x30x30cm) connected by open doorways. Prior to experimental social trials,
583 mice were habituated to the apparatus and allowed to freely explore all three chambers for 5 minutes. At
584 the end of the 5 minutes, mice were removed and placed in their home cage. A sex- and age-matched
585 stimulus mouse was then placed into a small empty cage in chamber 1 of the apparatus. The experimental
586 mouse was reintroduced to the center chamber (chamber 2) of the apparatus and recorded while freely

587 exploring for 10 minutes. The time spent in the chamber with the stimulus mouse (chamber 1) or the empty
588 chamber (chamber 3) was then measured.

589

590 *Fixed Minimum Interval (FMI)*

591 Twenty-four adult mice (12 *Slc32A1:Cre* mice: 5 males, 7 females; 12 *caMek1, Slc32A1:Cre* mice:
592 6 males, 6 females) were kept on a 12-hour reverse light-dark cycle. Animals had free access to water in
593 their home cages, but access to food was gradually reduced in the week prior to behavioral training, where
594 1 hr of food access was provided 30 min after the end of each daily training session. Body weights were
595 maintained such that mice lost no more than 15% of starting body weight. Behavioral testing was conducted
596 in eight MED Associates (St. Albans, VT, USA) modular test chambers (240 mm length × 200 mm width
597 × 165 mm height; ENV-307W). Each chamber was enclosed in a sound- and light-attenuating cabinet
598 (ENV-022V) equipped with a fan for ventilation that provided masking noise of approximately 60dB
599 (ENV-025-F28). The back wall and hinged front door of each chamber were made of Plexiglas. The side
600 walls of the chamber were made of aluminum, and the right wall contained the manipulanda and reward
601 receptacle. The floor was composed of thin metal bars. A circular reward receptacle was positioned in the
602 center of the front panel and equipped with a head entry detector (ENV-302HD), a liquid dipper (ENV-
603 302W-S), and a yellow LED (ENV-321W). The reward receptacle was flanked by a nose-poke device
604 including an LED-illuminator (ENV-314M). The chamber was fitted with a house light (ENV-315W) at
605 ceiling level above the back wall (ENV-323AW) and a 4.5kHz tone generator (ENV-323HAM).
606 Experimental programs were arranged via a MED PC interface connected to a PC controlled by MED-PC
607 IV software. All behavioral sessions were 30 min long, including a 3-min warm-up period during which no
608 stimuli were activated.

609 *Reinforcement Training and Autoshaping.* Mice were first trained to obtain 0.1 cc of diluted
610 sweetened condensed milk from the liquid dipper (the reinforcer) in the reward receptacle. Following the
611 3-min warmup period, a reinforcer was made available, followed by consistent reinforcer delivery at

612 variable, pseudo-randomly selected inter-trial intervals (ITIs) for the remainder of the session (mean = 45
613 s). No stimuli were activated during ITIs. When the dipper was activated and a reinforcer was available, a
614 2.9-kHz tone, the head-entry LED, and the house light were turned on. The reinforcer remained available
615 until it was obtained by the mouse, which deactivated the 2.9-kHz tone, the LED, and house light. The
616 dipper remains activated for 2.5s after the mouse obtains the reinforcer. Following 5 sessions of
617 reinforcement training, the procedure was modified for 5 autoshaping sessions which, in the last 8s of
618 each ITI, the LED inside of the nose-poke device was turned on. The nose-poke LED was then turned off
619 and reinforcement was delivered as described. If the mouse nose-poked the device during the time when
620 the LED was on, it was turned off and reinforcement was delivered immediately. The autoshaping
621 procedure was then modified for another 5 sessions such that reinforcement delivery was contingent upon
622 a single nose-poke to the nose-poke device when its LED was illuminated and the ITI was reduced to 10s.

623 *Fixed-Minimum Interval Training.* Mice were then trained on the fixed-minimum interval (FMI)
624 schedule. After the 3-min warmup period, the houselight was deactivated. A nose-poke (*initiating*
625 *response*) activated the nose-poke LED and marked the beginning of the inter-response time (IRT). A
626 subsequent head entry into the reward receptacle (*terminating response*) terminated the IRT.
627 Reinforcement was delivered only if the IRT was longer than the criterion time, which was dependent
628 upon the FMI schedule. IRTs shorter than the criterion time terminated without reinforcement,
629 deactivated the nose-poke LED, and another trial could be immediately initiated. IRTs greater than or
630 equal to the criterion time resulted in delivery of reward, deactivation of the nose-poke LED, a 2.5s
631 duration 2.9kHz tone, and subsequent removal of the liquid dipper. Houselights were then activated for a
632 10s ITI, after which houselight deactivation indicated a new trial could be initiated via nose-poke. The
633 time between the end of the ITI and the nose-poke initiating response was measured and termed the
634 *latency to initiate* (LTI). All mice were initially trained on an FMI schedule with a criterion time of 0.5s
635 (FMI 0.5s) until stability was achieved. The FMI 0.5s condition was implemented to acclimate mice to
636 the task and is not used to evaluate response inhibition capacity. Performance was considered stable when
637 a non-significant linear regression for mean median IRTs across 5 consecutive sessions was achieved,

638 using a significance criterion of .05. Following stability on the FMI 0.5s schedule, subjects experience
639 FMI 2s, 4s, and 8s. Each subject was trained to stability.

640 *Data Analysis.* Four parameters were tracked on a session-by-session basis: median latency-to-
641 initiate trials (LTI), median inter-response time (IRT), the coefficient of quartile variation (CQV) of IRTs
642 (difference between 1st and 3rd quartile divided by their sum), and the number of obtained reinforcers
643 (ORs). The acquisition phase of each parameter was defined as the mean performance during the first five
644 sessions of each schedule, while the asymptote was defined as the mean during the last five sessions.
645 ANOVAs were conducted to assess statistical significance of time and genotype on FMI schedule and
646 Student's *t*-tests were conducted to examine parameter differences based on genotype.

647 **References**

- 648 Adviento, B., Corbin, I.L., Widjaja, F., Desachy, G., Enrique, N., Rosser, T., Risi, S., Marco, E.J., Hendren,
649 R.L., Bearden, C.E., et al. (2014). Autism traits in the RASopathies. *J Med Genet* 51, 10-20.
- 650 Alessi, D.R., Saito, Y., Campbell, D.G., Cohen, P., Sithanandam, G., Rapp, U., Ashworth, A., Marshall,
651 C.J., and Cowley, S. (1994). Identification of the sites in MAP kinase kinase-1 phosphorylated by
652 p74raf-1. *EMBO J* 13, 1610-1619.
- 653 Anastasaki, C., and Gutmann, D. (2014). Neuronal NF1/RAS regulation of cyclic AMP requires atypical
654 PKC activation. *Human Molecular Genetics* 23, 6712-6721.
- 655 Anderson, T.R., Huguenard, J.R., Prince, D.A. (2010) Differential effects of Na⁺-K⁺ ATPase blockade on
656 cortical layer V neurons. *J Physiol.* 588,4401-14.
- 657 Aoidi, R., Houde, N., Landry-Truchon, K., Holter, M., Jacquet, K., Charron, L., Krishnaswami, S., Yu, B.,
658 Rauen, K., Bisson, N., et al. (2018). Mek1(Y130C) mice recapitulate aspects of human cardio-facio-
659 cutaneous syndrome. *Disease Models & Mechanisms* 11.
- 660 Bae, M.H., Bissonette, G.B., Mars, W.M., Michalopoulos, G.K., Achim, C.L., Depireux, D.A., and Powell,
661 E.M. (2010). Hepatocyte growth factor (HGF) modulates GABAergic inhibition and seizure
662 susceptibility. *Exp Neurol* 221, 129-135.
- 663 Berryer, M.H., Chattopadhyaya, B., Xing, P., Riebe, I., Bosoi, C., Sanon, N., Antoine-Bertrand, J.,
664 Lévesque, M., Avoli, M., Hamdan, F.F., et al. (2016). Decrease of SYNGAP1 in GABAergic cells
665 impairs inhibitory synapse connectivity, synaptic inhibition and cognitive function. *Nat Commun* 7,
666 13340.
- 667 Bitanhirwe, B.K., and Woo, T.U. (2014). Perineuronal nets and schizophrenia: the importance of neuronal
668 coatings. *Neurosci Biobehav Rev* 45, 85-99.
- 669 Bizarro, L., Murtagh, C., and Stolerman, I. (2003). Differing effects of nicotine, amphetamine and caffeine
670 on performance of a 5-choice serial reaction time task. *Journal of Psychopharmacology* 17, A31-A31.

671 Brown, J., Diggs-Andrews, K., Gianino, S., and Gutmann, D. (2012). Neurofibromatosis-1 heterozygosity
672 impairs CNS neuronal morphology in a cAMP/PKA/ROCK-dependent manner. *Molecular and Cellular*
673 *Neuroscience* 49, 13-22.

674 Bueno, O.F., De Windt, L.J., Tymitz, K.M., Witt, S.A., Kimball, T.R., Klevitsky, R., Hewett, T.E., Jones,
675 S.P., Lefer, D.J., Peng, C.F., et al. (2000). The MEK1-ERK1/2 signaling pathway promotes
676 compensated cardiac hypertrophy in transgenic mice. *EMBO J* 19, 6341-6350.

677 Cabungcal, J.H., Steullet, P., Morishita, H., Kraftsik, R., Cuenod, M., Hensch, T.K., and Do, K.Q. (2013).
678 Perineuronal nets protect fast-spiking interneurons against oxidative stress. *Proc Natl Acad Sci U S A*
679 110, 9130-9135.

680 Cagnol, S., and Chambard, J.C. (2010). ERK and cell death: mechanisms of ERK-induced cell death--
681 apoptosis, autophagy and senescence. *FEBS J* 277, 2-21.

682 Cancedda, L., Fiumelli, H., Chen, K., and Poo, M. (2007). Excitatory GABA action is essential for
683 morphological maturation of cortical neurons in vivo. *Journal of Neuroscience* 27, 5224-5235.

684 Cancedda, L., Putignano, E., Impey, S., Maffei, L., Ratto, G.M., and Pizzorusso, T. (2003). Patterned vision
685 causes CRE-mediated gene expression in the visual cortex through PKA and ERK. *J Neurosci* 23, 7012-
686 7020.

687 Chao, H.T., Chen, H., Samaco, R.C., Xue, M., Chahrour, M., Yoo, J., Neul, J.L., Gong, S., Lu, H.C., Heintz,
688 N., et al. (2010). Dysfunction in GABA signalling mediates autism-like stereotypies and Rett syndrome
689 phenotypes. *Nature* 468, 263-269.

690 Chattopadhyaya, B., Di Cristo, G., Higashiyama, H., Knott, G.W., Kuhlman, S.J., Welker, E., and Huang,
691 Z.J. (2004). Experience and activity-dependent maturation of perisomatic GABAergic innervation in
692 primary visual cortex during a postnatal critical period. *J Neurosci* 24, 9598-9611.

693 Chattopadhyaya, B., Di Cristo, G., Wu, C.Z., Knott, G., Kuhlman, S., Fu, Y., Palmiter, R.D., and Huang,
694 Z.J. (2007). GAD67-mediated GABA synthesis and signaling regulate inhibitory synaptic innervation
695 in the visual cortex. *Neuron* 54, 889-903.

696 Clement, J.P., Aceti, M., Creson, T.K., Ozkan, E.D., Shi, Y., Reish, N.J., Almonte, A.G., Miller, B.H.,
697 Wiltgen, B.J., Miller, C.A., et al. (2012). Pathogenic SYNGAP1 mutations impair cognitive
698 development by disrupting maturation of dendritic spine synapses. *Cell* 151, 709-723.

699 Cowley, S., Paterson, H., Kemp, P., and Marshall, C.J. (1994). Activation of MAP kinase kinase is
700 necessary and sufficient for PC12 differentiation and for transformation of NIH 3T3 cells. *Cell* 77, 841-
701 852.

702 Cui, Y., Costa, R., Murphy, G., Elgersma, Y., Zhu, Y., Gutmann, D., Parada, L., Mody, I., and Silva, A.
703 (2008). Neurofibromin Regulation of ERK Signaling Modulates GABA Release and Learning. *Cell*
704 135, 549-560.

705 Denaxa, M., Neves, G., Rabinowitz, A., Kemlo, S., Liodis, P., Burrone, J., and Pachnis, V. (2018).
706 Modulation of Apoptosis Controls Inhibitory Interneuron Number in the Cortex. *Cell Rep* 22, 1710-
707 1721.

708 Digilio, M.C., Lepri, F., Baban, A., Dentici, M.L., Versacci, P., Capolino, R., Ferese, R., De Luca, A.,
709 Tartaglia, M., Marino, B., et al. (2011). RASopathies: Clinical Diagnosis in the First Year of Life. *Mol*
710 *Syndromol* 1, 282-289.

711 Doughty, A.H., and Richards, J.B. (2002). Effects of reinforcer magnitude on responding under differential-
712 reinforcement-of-low-rate schedules of rats and pigeons. *J Exp Anal Behav* 78, 17-30.

713 Ehrman, L., Nardini, D., Ehrman, S., Rizvi, T., Gulick, J., Krenz, M., Dasgupta, B., Robbins, J., Ratner, N.,
714 Nakafuku, M., et al. (2014). The Protein Tyrosine Phosphatase Shp2 Is Required for the Generation of
715 Oligodendrocyte Progenitor Cells and Myelination in the Mouse Telencephalon. *Journal of*
716 *Neuroscience* 34, 3767-3778.

717 El Idrissi, A., Ding, X.H., Scalia, J., Trenkner, E., Brown, W.T., and Dobkin, C. (2005). Decreased
718 GABA(A) receptor expression in the seizure-prone fragile X mouse. *Neurosci Lett* 377, 141-146.

719 Fazzari, P., Paternain, A.V., Valiente, M., Pla, R., Luján, R., Lloyd, K., Lerma, J., Marín, O., and Rico, B.
720 (2010). Control of cortical GABA circuitry development by Nrg1 and ErbB4 signalling. *Nature* 464,
721 1376-1380.

- 722 Fino, E., Packer, A.M., and Yuste, R. (2013). The logic of inhibitory connectivity in the neocortex.
723 *Neuroscientist* 19, 228-237.
- 724 Flames, N., Long, J., Garratt, A., Fischer, T., Gassmann, M., Birchmeier, C., Lai, C., Rubenstein, J., and
725 Marin, O. (2004). Short- and long-range attraction of cortical GABAergic interneurons by Neuregulin-
726 1. *Neuron* 44, 251-261.
- 727 Fowke, T.M., Galinsky, R., Davidson, J.O., Wassink, G., Karunasinghe, R.N., Prasad, J.D., Bennet, L.,
728 Gunn, A.J., and Dean, J.M. (2018). Loss of interneurons and disruption of perineuronal nets in the
729 cerebral cortex following hypoxia-ischaemia in near-term fetal sheep. *Sci Rep* 8, 17686.
- 730 Gabay, Y., Shahbani-Khateb, E., and Mendelsohn, A. (2018). Feedback Timing Modulates Probabilistic
731 Learning in Adults with ADHD. *Sci Rep* 8, 15524.
- 732 Galtrey, C.M., and Fawcett, J.W. (2007). The role of chondroitin sulfate proteoglycans in regeneration and
733 plasticity in the central nervous system. *Brain Res Rev* 54, 1-18.
- 734 Garg, S., Lehtonen, A., Huson, S.M., Emsley, R., Trump, D., Evans, D.G., and Green, J. (2013). Autism
735 and other psychiatric comorbidity in neurofibromatosis type 1: evidence from a population-based study.
736 *Dev Med Child Neurol* 55, 139-145.
- 737 Gauthier, A., Furstoss, O., Araki, T., Chan, R., Neel, B., Kaplan, D., and Miller, F. (2007). Control of CNS
738 cell-fate decisions by SHP-2 and its dysregulation in Noonan syndrome. *Neuron* 54, 245-262.
- 739 Gelman, D., Martini, F., Nobrega-Pereira, S., Pierani, A., Kessar, N., and Marin, O. (2009). The
740 Embryonic Preoptic Area Is a Novel Source of Cortical GABAergic Interneurons. *Journal of*
741 *Neuroscience* 29, 9380-9389.
- 742 Gelman, D.M., and Marín, O. (2010). Generation of interneuron diversity in the mouse cerebral cortex. *Eur*
743 *J Neurosci* 31, 2136-2141.
- 744 Goldberg, E., Jeong, H., Kruglikov, I., Tremblay, R., Lazarenko, R., and Rudy, B. (2011). Rapid
745 Developmental Maturation of Neocortical FS Cell Intrinsic Excitability. *Cerebral Cortex* 21, 666-682.

- 746 Green, T., Naylor, P.E., and Davies, W. (2017). Attention deficit hyperactivity disorder (ADHD) in
747 phenotypically similar neurogenetic conditions: Turner syndrome and the RASopathies. *J Neurodev*
748 *Disord* 9, 25.
- 749 Hensch, T. (2005a). Critical period mechanisms in developing visual cortex. *Current Topics in*
750 *Developmental Biology*, Vol 69 69, 215-+.
- 751 Hensch, T.K. (2005b). Critical period plasticity in local cortical circuits. *Nat Rev Neurosci* 6, 877-888.
- 752 Hill, J.C., Herbst, K., and Sanabria, F. (2012). Characterizing operant hyperactivity in the Spontaneously
753 Hypertensive Rat. *Behav Brain Funct* 8, 5.
- 754 Holter, M.C., Hewitt, L.T., Koebele, S.V., Judd, J.M., Xing, L., Bimonte-Nelson, H.A., Conrad, C.D.,
755 Araki, T., Neel, B.G., Snider, W.D., et al. (2019). The Noonan Syndrome-linked Raf1L613V mutation
756 drives increased glial number in the mouse cortex and enhanced learning. *PLoS Genet* 15, e1008108.
- 757 Hrvatin, S., Hochbaum, D.R., Nagy, M.A., Cicconet, M., Robertson, K., Cheadle, L., Zilionis, R., Ratner,
758 A., Borges-Monroy, R., Klein, A.M., et al. (2018). Single-cell analysis of experience-dependent
759 transcriptomic states in the mouse visual cortex. *Nat Neurosci* 21, 120-129.
- 760 Ishii, A., Furusho, M., and Bansal, R. (2013). Sustained Activation of ERK1/2 MAPK in Oligodendrocytes
761 and Schwann Cells Enhances Myelin Growth and Stimulates Oligodendrocyte Progenitor Expansion.
762 *Journal of Neuroscience* 33, 175-186.
- 763 Johnson, E.M., Ishak, A.D., Naylor, P.E., Stevenson, D.A., Reiss, A.L., and Green, T. (2019). PTPN11
764 Gain-of-Function Mutations Affect the Developing Human Brain, Memory, and Attention. *Cereb*
765 *Cortex* 29, 2915-2923.
- 766 Kelsom, C., and Lu, W. (2013). Development and specification of GABAergic cortical interneurons. *Cell*
767 *Biosci* 3, 19.
- 768 Kessar, N., Magno, L., Rubin, A.N., and Oliveira, M.G. (2014). Genetic programs controlling cortical
769 interneuron fate. *Curr Opin Neurobiol* 26, 79-87.
- 770 Klesse, L.J., Meyers, K.A., Marshall, C.J., and Parada, L.F. (1999). Nerve growth factor induces survival
771 and differentiation through two distinct signaling cascades in PC12 cells. *Oncogene* 18, 2055-2068.

772 Krencik, R., Hokanson, K.C., Narayan, A.R., Dvornik, J., Rooney, G.E., Rauen, K.A., Weiss, L.A.,
773 Rowitch, D.H., and Ullian, E.M. (2015). Dysregulation of astrocyte extracellular signaling in Costello
774 syndrome. *Sci Transl Med* 7, 286ra266.

775 Krens, S.F., Spaink, H.P., and Snaar-Jagalska, B.E. (2006). Functions of the MAPK family in vertebrate-
776 development. *FEBS Lett* 580, 4984-4990.

777 Krenz, M., Gulick, J., Osinska, H.E., Colbert, M.C., Molkentin, J.D., and Robbins, J. (2008). Role of
778 ERK1/2 signaling in congenital valve malformations in Noonan syndrome. *Proc Natl Acad Sci U S A*
779 105, 18930-18935.

780 Krishnan, K., Wang, B.S., Lu, J., Wang, L., Maffei, A., Cang, J., and Huang, Z.J. (2015). MeCP2 regulates
781 the timing of critical period plasticity that shapes functional connectivity in primary visual cortex. *Proc*
782 *Natl Acad Sci U S A* 112, E4782-4791.

783 Krueger, D.D., Osterweil, E.K., Chen, S.P., Tye, L.D., and Bear, M.F. (2011). Cognitive dysfunction and
784 prefrontal synaptic abnormalities in a mouse model of fragile X syndrome. *Proc Natl Acad Sci U S A*
785 108, 2587-2592.

786 Kumar, R.A., KaraMohamed, S., Sudi, J., Conrad, D.F., Brune, C., Badner, J.A., Gilliam, T.C., Nowak,
787 N.J., Cook, E.H., Dobyns, W.B., et al. (2008). Recurrent 16p11.2 microdeletions in autism. *Hum Mol*
788 *Genet* 17, 628-638.

789 Lajiness, J.D., Snider, P., Wang, J., Feng, G.S., Krenz, M., and Conway, S.J. (2014). SHP-2 deletion in
790 postmigratory neural crest cells results in impaired cardiac sympathetic innervation. *Proc Natl Acad*
791 *Sci U S A* 111, E1374-1382.

792 Lavdas, A.A., Grigoriou, M., Pachnis, V., and Parnavelas, J.G. (1999). The medial ganglionic eminence
793 gives rise to a population of early neurons in the developing cerebral cortex. *J Neurosci* 19, 7881-7888.

794 Li, X., Newbern, J., Wu, Y., Morgan-Smith, M., Zhong, J., Charron, J., and Snider, W. (2012). MEK Is a
795 Key Regulator of Gliogenesis in the Developing Brain. *Neuron* 75, 1035-1050.

796 Lim, L., Mi, D., Llorca, A., and Marín, O. (2018). Development and Functional Diversification of Cortical
797 Interneurons. *Neuron* 100, 294-313.

798 Madisen, L., Zwingman, T.A., Sunkin, S.M., Oh, S.W., Zariwala, H.A., Gu, H., Ng, L.L., Palmiter, R.D.,
799 Hawrylycz, M.J., Jones, A.R., et al. (2010). A robust and high-throughput Cre reporting and
800 characterization system for the whole mouse brain. *Nat Neurosci* 13, 133-140.

801 Mardinly, A.R., Spiegel, I., Patrizi, A., Centofante, E., Bazinet, J.E., Tzeng, C.P., Mandel-Brehm, C.,
802 Harmin, D.A., Adesnik, H., Fagiolini, M., et al. (2016). Sensory experience regulates cortical inhibition
803 by inducing IGF1 in VIP neurons. *Nature* 531, 371-375.

804 Marin, O., and Rubenstein, J. (2001). A long, remarkable journey: Tangential migration in the
805 telencephalon. *Nature Reviews Neuroscience* 2, 780-790.

806 Marin, O., and Rubenstein, J. (2003). Cell migration in the forebrain. *Annual Review of Neuroscience* 26,
807 441-483.

808 Martin, P., and Pognonec, P. (2010). ERK and cell death: cadmium toxicity, sustained ERK activation and
809 cell death. *FEBS J* 277, 39-46.

810 Mattar, P., Langevin, L.M., Markham, K., Klenin, N., Shivji, S., Zinyk, D., and Schuurmans, C. (2008).
811 Basic helix-loop-helix transcription factors cooperate to specify a cortical projection neuron identity.
812 *Mol Cell Biol* 28, 1456-1469.

813 Mayer, C., Hafemeister, C., Bandler, R.C., Machold, R., Batista Brito, R., Jaglin, X., Allaway, K., Butler,
814 A., Fishell, G., and Satija, R. (2018). Developmental diversification of cortical inhibitory interneurons.
815 *Nature* 555, 457-462.

816 McCormick, D.A., Connors, B.W., Lighthall, J.W., Prince, D.A. (1985) Comparative electrophysiology of
817 pyramidal and sparsely spiny stellate neurons of the neocortex. *J Neurophysiol.* 54:782-806.

818 Mi, D., Li, Z., Lim, L., Li, M., Moissidis, M., Yang, Y., Gao, T., Hu, T.X., Pratt, T., Price, D.J., et al.
819 (2018). Early emergence of cortical interneuron diversity in the mouse embryo. *Science* 360, 81-85.

820 Miguel, C.S., Chaim-Avancini, T.M., Silva, M.A., and Louzã, M.R. (2015). Neurofibromatosis type 1 and
821 attention deficit hyperactivity disorder: a case study and literature review. *Neuropsychiatr Dis Treat* 11,
822 815-821.

823 Monory, K., Massa, F., Egertová, M., Eder, M., Blaudzun, H., Westenbroek, R., Kelsch, W., Jacob, W.,
824 Marsch, R., Ekker, M., et al. (2006). The endocannabinoid system controls key epileptogenic circuits
825 in the hippocampus. *Neuron* 51, 455-466.

826 Morishita, H., Cabungcal, J., Chen, Y., Do, K., and Hensch, T. (2015). Prolonged Period of Cortical
827 Plasticity upon Redox Dysregulation in Fast-Spiking Interneurons. *Biological Psychiatry* 78, 396-402.

828 Nateri, A.S., Raivich, G., Gebhardt, C., Da Costa, C., Naumann, H., Vreugdenhil, M., Makwana, M.,
829 Brandner, S., Adams, R.H., Jefferys, J.G., et al. (2007). ERK activation causes epilepsy by stimulating
830 NMDA receptor activity. *EMBO J* 26, 4891-4901.

831 Nichols, J., Bjorklund, G.R., Newbern, J., and Anderson, T. (2018). Parvalbumin fast-spiking interneurons
832 are selectively altered by paediatric traumatic brain injury. *J Physiol* 596, 1277-1293.

833 Okaty, B., Miller, M., Sugino, K., Hempel, C., and Nelson, S. (2009). Transcriptional and
834 Electrophysiological Maturation of Neocortical Fast-Spiking GABAergic Interneurons. *Journal of*
835 *Neuroscience* 29, 7040-7052.

836 Ozkan, E.D., Creson, T.K., Kramár, E.A., Rojas, C., Seese, R.R., Babyan, A.H., Shi, Y., Lucero, R., Xu,
837 X., Noebels, J.L., et al. (2014). Reduced cognition in *Syngap1* mutants is caused by isolated damage
838 within developing forebrain excitatory neurons. *Neuron* 82, 1317-1333.

839 Paluszkiwicz, S.M., Martin, B.S., and Huntsman, M.M. (2011). Fragile X syndrome: the GABAergic
840 system and circuit dysfunction. *Dev Neurosci* 33, 349-364.

841 Parnavelas, J.G. (2000). The origin and migration of cortical neurones: new vistas. *Trends Neurosci* 23,
842 126-131.

843 Paul, A., Crow, M., Raudales, R., He, M., Gillis, J., and Huang, Z.J. (2017). Transcriptional Architecture
844 of Synaptic Communication Delineates GABAergic Neuron Identity. *Cell* 171, 522-539.e520.

845 Perrinjaquet, M., Sjostrand, D., Moliner, A., Zechel, S., Lamballe, F., Maina, F., and Ibanez, C. (2011).
846 MET signaling in GABAergic neuronal precursors of the medial ganglionic eminence restricts GDNF
847 activity in cells that express GFR alpha 1 and a new transmembrane receptor partner. *Journal of Cell*
848 *Science* 124, 2797-2805.

- 849 Pham, T.A., Graham, S.J., Suzuki, S., Barco, A., Kandel, E.R., Gordon, B., and Lickey, M.E. (2004). A
850 semi-persistent adult ocular dominance plasticity in visual cortex is stabilized by activated CREB.
851 *Learn Mem* 11, 738-747.
- 852 Pierpont, E., Hudock, R., Foy, A., Semrud-Clikeman, M., Pierpont, M., Berry, S., Shanley, R., Rubin, N.,
853 Sommer, K., and Moertel, C. (2018). Social skills in children with RASopathies: a comparison of
854 Noonan syndrome and neurofibromatosis type 1. *Journal of Neurodevelopmental Disorders* 10.
- 855 Pierpont, E., Tworog-Dube, E., and Roberts, A. (2015). Attention skills and executive functioning in
856 children with Noonan syndrome and their unaffected siblings. *Developmental Medicine and Child
857 Neurology* 57, 385-392.
- 858 Pizzorusso, T., Medini, P., Berardi, N., Chierzi, S., Fawcett, J.W., and Maffei, L. (2002). Reactivation of
859 ocular dominance plasticity in the adult visual cortex. *Science* 298, 1248-1251.
- 860 Pozas, E., and Ibanez, C. (2005). GDNF and GFR alpha 1 promote differentiation and tangential migration
861 of cortical GABAergic neurons. *Neuron* 45, 701-713.
- 862 Pucilowska, J., Puzerey, P., Karlo, J., Galan, R., and Landreth, G. (2012). Disrupted ERK Signaling during
863 Cortical Development Leads to Abnormal Progenitor Proliferation, Neuronal and Network Excitability
864 and Behavior, Modeling Human Neuro-Cardio-Facial-Cutaneous and Related Syndromes. *Journal of
865 Neuroscience* 32, 8663-8677.
- 866 Pucilowska, J., Vithayathil, J., Pagani, M., Kelly, C., Karlo, J.C., Robol, C., Morella, I., Gozzi, A.,
867 Brambilla, R., and Landreth, G.E. (2018). Pharmacological Inhibition of ERK Signaling Rescues
868 Pathophysiology and Behavioral Phenotype Associated with 16p11.2 Chromosomal Deletion in Mice.
869 *J Neurosci* 38, 6640-6652.
- 870 Pucilowska, J., Vithayathil, J., Tavares, E., Kelly, C., Karlo, J., and Landreth, G. (2015). The 16p11.2
871 Deletion Mouse Model of Autism Exhibits Altered Cortical Progenitor Proliferation and Brain
872 Cytoarchitecture Linked to the ERK MAPK Pathway. *Journal of Neuroscience* 35, 3190-3200.
- 873 Rauen, K., Chakravarti, A., and Green, E. (2013). The RASopathies. *Annual Review of Genomics and
874 Human Genetics*, Vol 14 14, 355-369.

- 875 Rojas-Leguizamón, M., Baroja, J.L., Sanabria, F., and Orduña, V. (2018). Response-inhibition capacity in
876 spontaneously hypertensive and Wistar rats: acquisition of fixed minimum interval performance and
877 responsiveness to D-amphetamine. *Behav Pharmacol* 29, 668-675.
- 878 Rosato-Siri, M., Zambello, E., Mutinelli, C., Garbati, N., Benedetti, R., Aldegheri, L., Graziani, F.,
879 Virginio, C., Alvaro, G., and Large, C. (2015). A Novel Modulator of Kv3 Potassium Channels
880 Regulates the Firing of Parvalbumin-Positive Cortical Interneurons. *Journal of Pharmacology and*
881 *Experimental Therapeutics* 354, 251-260.
- 882 Rudy, B., Fishell, G., Lee, S., and Hjerling-Leffler, J. (2011). Three groups of interneurons account for
883 nearly 100% of neocortical GABAergic neurons. *Dev Neurobiol* 71, 45-61.
- 884 Rudy, B., and McBain, C. (2001). Kv3 channels: voltage-gated K⁺ channels designed for high-frequency
885 repetitive firing. *Trends in Neurosciences* 24, 517-526.
- 886 Samuels, I., Saitta, S., and Landreth, G. (2009). MAP'ing CNS Development and Cognition: An ERKsome
887 Process. *Neuron* 61, 160-167.
- 888 Sandberg, M., Taher, L., Hu, J., Black, B.L., Nord, A.S., and Rubenstein, J.L.R. (2018). Genomic analysis
889 of transcriptional networks directing progression of cell states during MGE development. *Neural Dev*
890 13, 21.
- 891 Seidman, L.J., Valera, E.M., Makris, N., Monuteaux, M.C., Boriel, D.L., Kelkar, K., Kennedy, D.N.,
892 Caviness, V.S., Bush, G., Alvardi, M., et al. (2006). Dorsolateral prefrontal and anterior cingulate cortex
893 volumetric abnormalities in adults with attention-deficit/hyperactivity disorder identified by magnetic
894 resonance imaging. *Biol Psychiatry* 60, 1071-1080.
- 895 Selby, L., Zhang, C., and Sun, Q.Q. (2007). Major defects in neocortical GABAergic inhibitory circuits in
896 mice lacking the fragile X mental retardation protein. *Neurosci Lett* 412, 227-232.
- 897 Sorg, B.A., Berretta, S., Blacktop, J.M., Fawcett, J.W., Kitagawa, H., Kwok, J.C., and Miquel, M. (2016).
898 Casting a Wide Net: Role of Perineuronal Nets in Neural Plasticity. *J Neurosci* 36, 11459-11468.

899 Southwell, D., Paredes, M., Galvao, R., Jones, D., Froemke, R., Sebe, J., Alfaro-Cervello, C., Tang, Y.,
900 Garcia-Verdugo, J., Rubenstein, J., et al. (2012). Intrinsically determined cell death of developing
901 cortical interneurons. *Nature* 491, 109-U172.

902 Stanco, A., Pla, R., Vogt, D., Chen, Y., Mandal, S., Walker, J., Hunt, R., Lindtner, S., Erdman, C., Pieper,
903 A., et al. (2014). NPAS1 Represses the Generation of Specific Subtypes of Cortical Interneurons.
904 *Neuron* 84, 940-953.

905 Steullet, P., Cabungcal, J.H., Coyle, J., Didriksen, M., Gill, K., Grace, A.A., Hensch, T.K., LaMantia, A.S.,
906 Lindemann, L., Maynard, T.M., et al. (2017). Oxidative stress-driven parvalbumin interneuron
907 impairment as a common mechanism in models of schizophrenia. *Mol Psychiatry* 22, 936-943.

908 Steward, O., Torre, E., Tomasulo, R., and Lothman, E. (1992). Seizures and the Regulation of Astroglial
909 Gene Expression. *Epilepsy Research*, 197-209.

910 Stringer, J. (1996). Repeated seizures increase GFAP and vimentin in the hippocampus. *Brain Research*
911 717, 147-153.

912 Suzuki, S., al-Noori, S., Butt, S.A., and Pham, T.A. (2004). Regulation of the CREB signaling cascade in
913 the visual cortex by visual experience and neuronal activity. *J Comp Neurol* 479, 70-83.

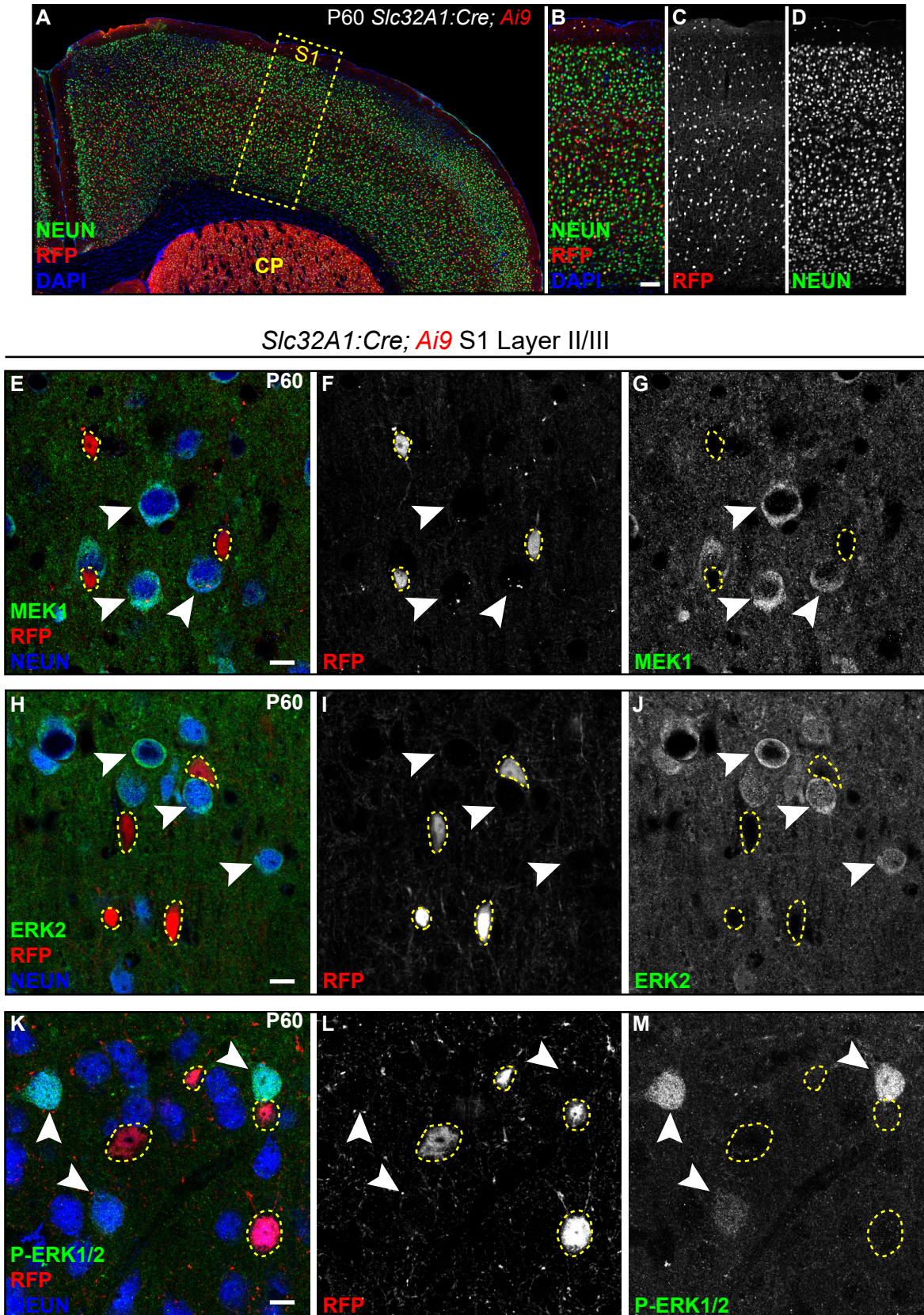
914 Tamamaki, N., Fujimori, K.E., and Takauji, R. (1997). Origin and route of tangentially migrating neurons
915 in the developing neocortical intermediate zone. *J Neurosci* 17, 8313-8323.

916 Tidyman, W., and Rauen, K. (2016). Pathogenetics of the RASopathies. *Human Molecular Genetics* 25,
917 R123-R132.

918 Tyssowski, K.M., DeStefino, N.R., Cho, J.H., Dunn, C.J., Poston, R.G., Carty, C.E., Jones, R.D., Chang,
919 S.M., Romeo, P., Wurzelmann, M.K., et al. (2018). Different Neuronal Activity Patterns Induce
920 Different Gene Expression Programs. *Neuron* 98, 530-546.e511.

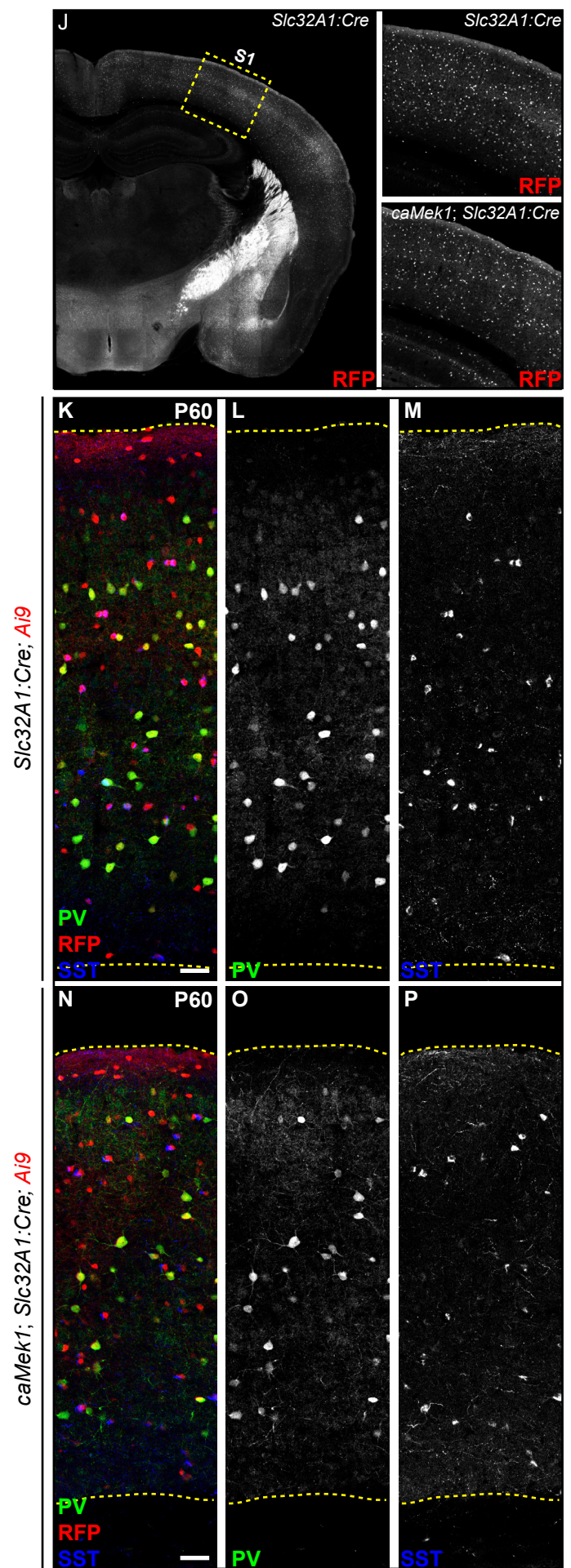
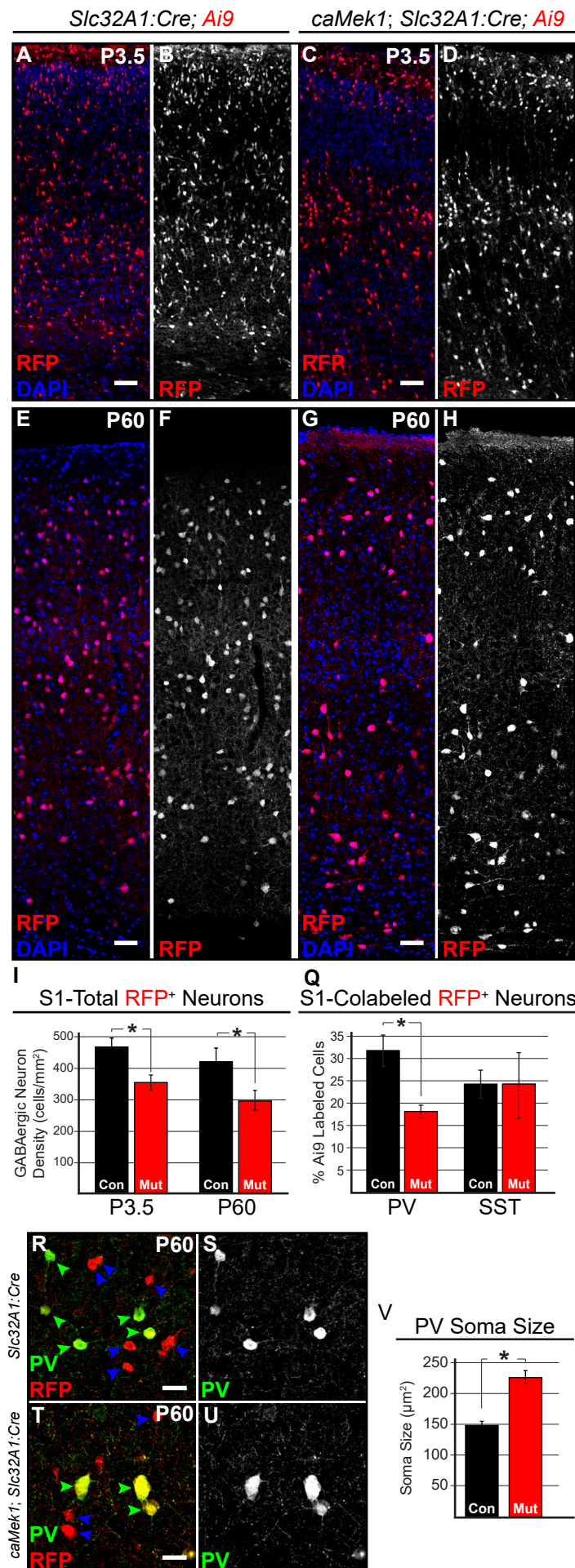
921 Ure, K., Lu, H., Wang, W., Ito-Ishida, A., Wu, Z., He, L.J., Sztainberg, Y., Chen, W., Tang, J., and Zoghbi,
922 H.Y. (2016). Restoration of Mecp2 expression in GABAergic neurons is sufficient to rescue multiple
923 disease features in a mouse model of Rett syndrome. *Elife* 5.

- 924 Vong, L., Ye, C., Yang, Z., Choi, B., Chua, S., and Lowell, B.B. (2011). Leptin action on GABAergic
925 neurons prevents obesity and reduces inhibitory tone to POMC neurons. *Neuron* 71, 142-154.
- 926 Vorstman, J.A., Staal, W.G., van Daalen, E., van Engeland, H., Hochstenbach, P.F., and Franke, L. (2006).
927 Identification of novel autism candidate regions through analysis of reported cytogenetic abnormalities
928 associated with autism. *Mol Psychiatry* 11, 1, 18-28.
- 929 Walsh, K.S., Vélez, J.I., Kardel, P.G., Imas, D.M., Muenke, M., Packer, R.J., Castellanos, F.X., and Acosta,
930 M.T. (2013). Symptomatology of autism spectrum disorder in a population with neurofibromatosis type
931 1. *Dev Med Child Neurol* 55, 131-138.
- 932 Watterson, E., Mazur, G.J., and Sanabria, F. (2015). Validation of a method to assess ADHD-related
933 impulsivity in animal models. *J Neurosci Methods* 252, 36-47.
- 934 Wichterle, H., Garcia-Verdugo, J.M., Herrera, D.G., and Alvarez-Buylla, A. (1999). Young neurons from
935 medial ganglionic eminence disperse in adult and embryonic brain. *Nat Neurosci* 2, 461-466.
- 936 Wichterle, H., Turnbull, D., Nery, S., Fishell, G., and Alvarez-Buylla, A. (2001). In utero fate mapping
937 reveals distinct migratory pathways and fates of neurons born in the mammalian basal forebrain.
938 *Development* 128, 3759-3771.
- 939 Wonders, C., and Anderson, S. (2006). The origin and specification of cortical interneurons. *Nature*
940 *Reviews Neuroscience* 7, 687-696.
- 941 Xing, L., Larsen, R., Bjorklund, G., Li, X., Wu, Y., Philpot, B., Snider, W., and Newbern, J. (2016). Layer
942 specific and general requirements for ERK/MAPK signaling in the developing neocortex. *Elife* 5.
- 943 Yoon, G., Rosenberg, J., Blaser, S., and Rauen, K. (2007). Neurological complications of cardio-facio-
944 cutaneous syndrome. *Developmental Medicine and Child Neurology* 49, 894-899.
- 945 Zhang, Z.W., Zak, J.D., and Liu, H. (2010). MeCP2 is required for normal development of GABAergic
946 circuits in the thalamus. *J Neurophysiol* 103, 2470-2481.



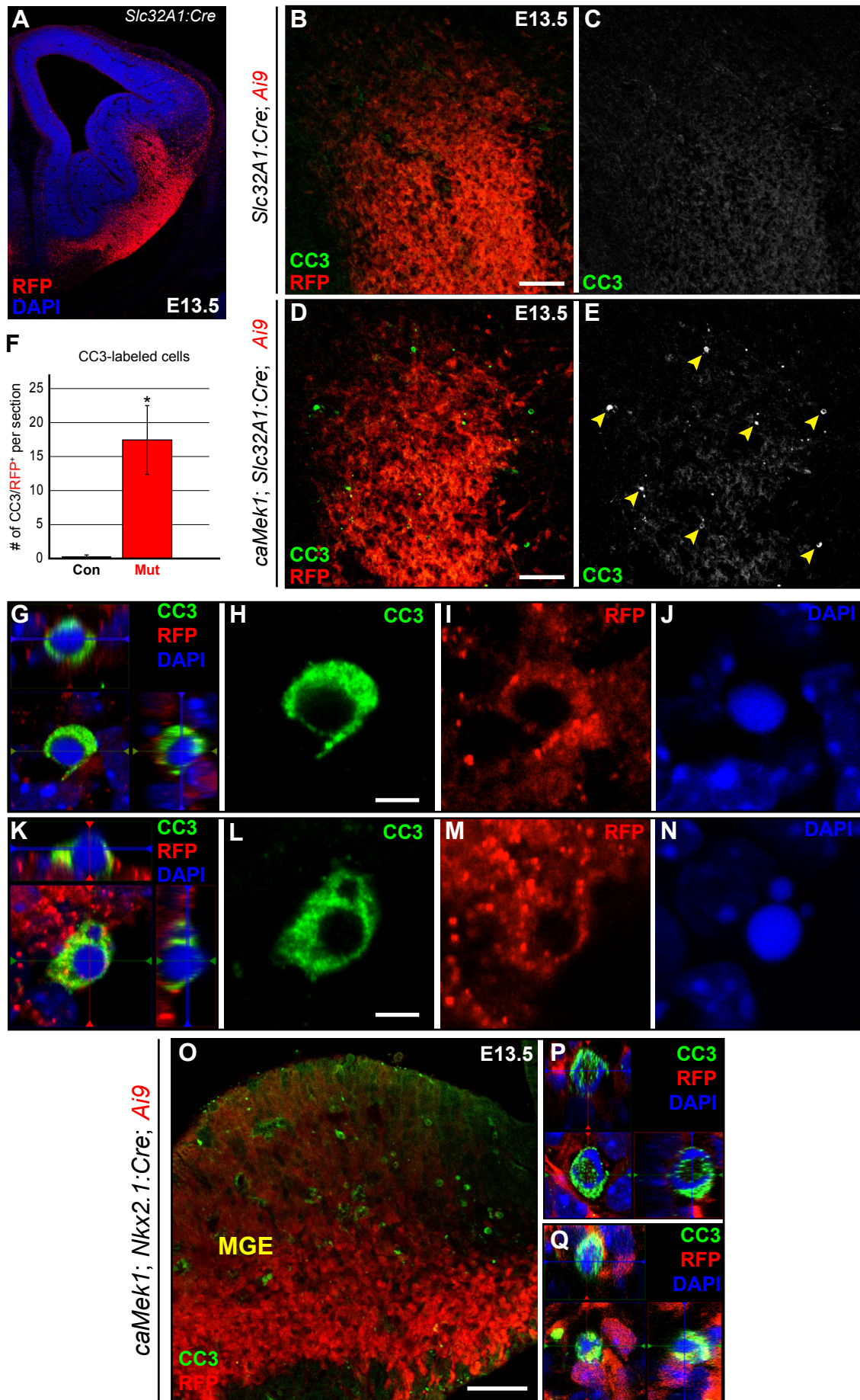
Primary Somatosensory Cortex

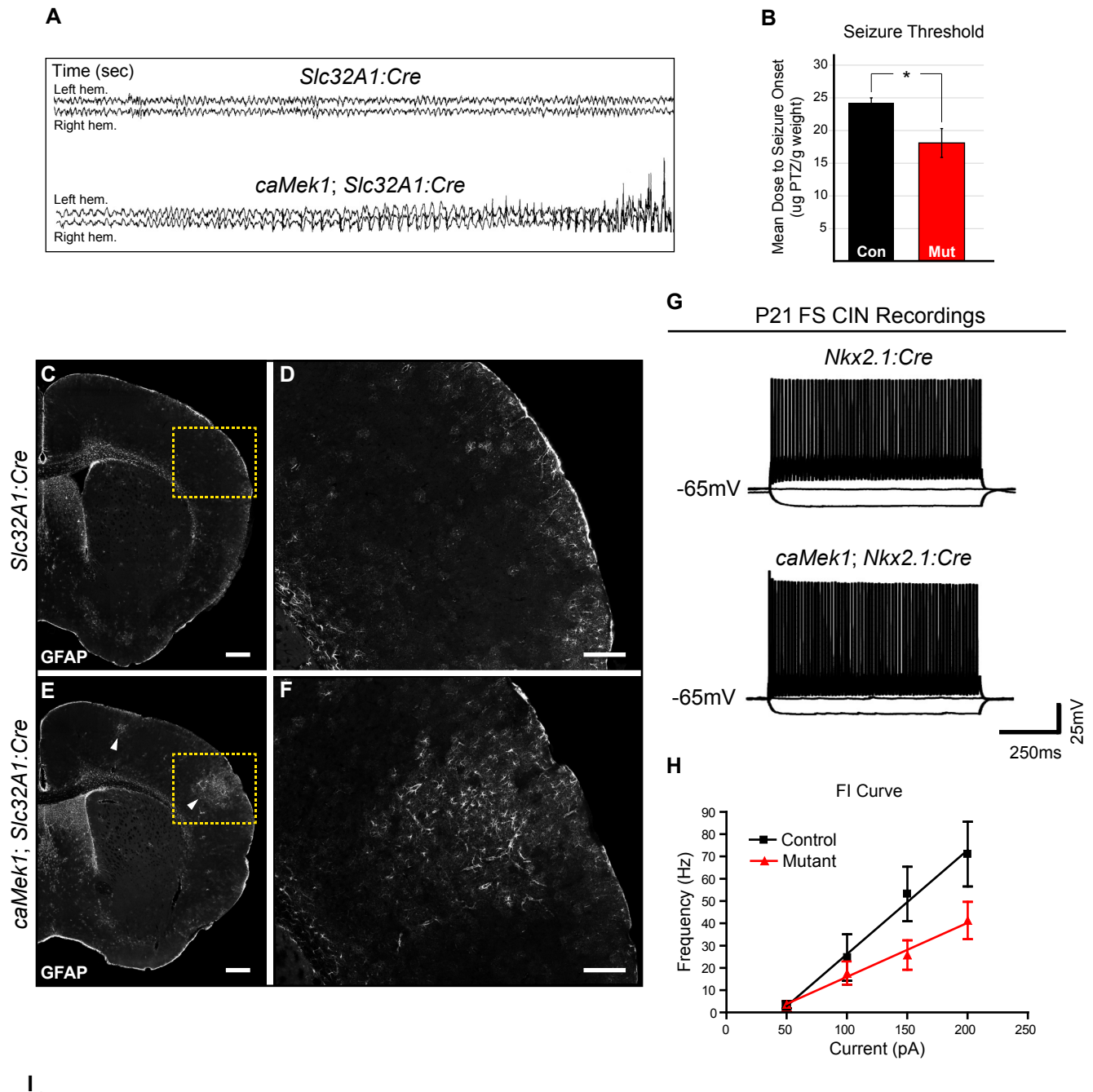
Figure 2



E13.5 Ganglionic Eminences (GE)

Figure 3





Layer II/III Perisomatic GABAergic Synapses

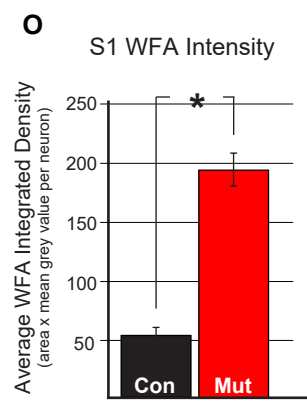
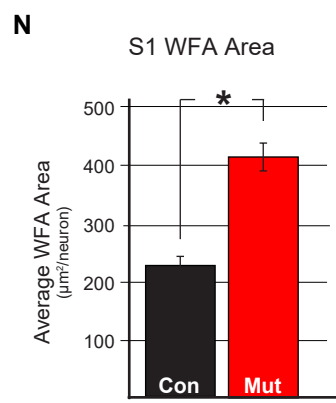
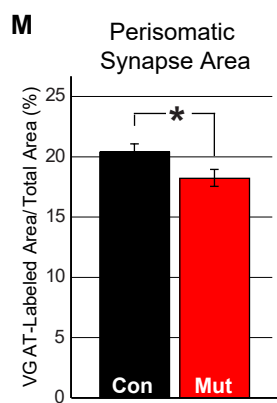
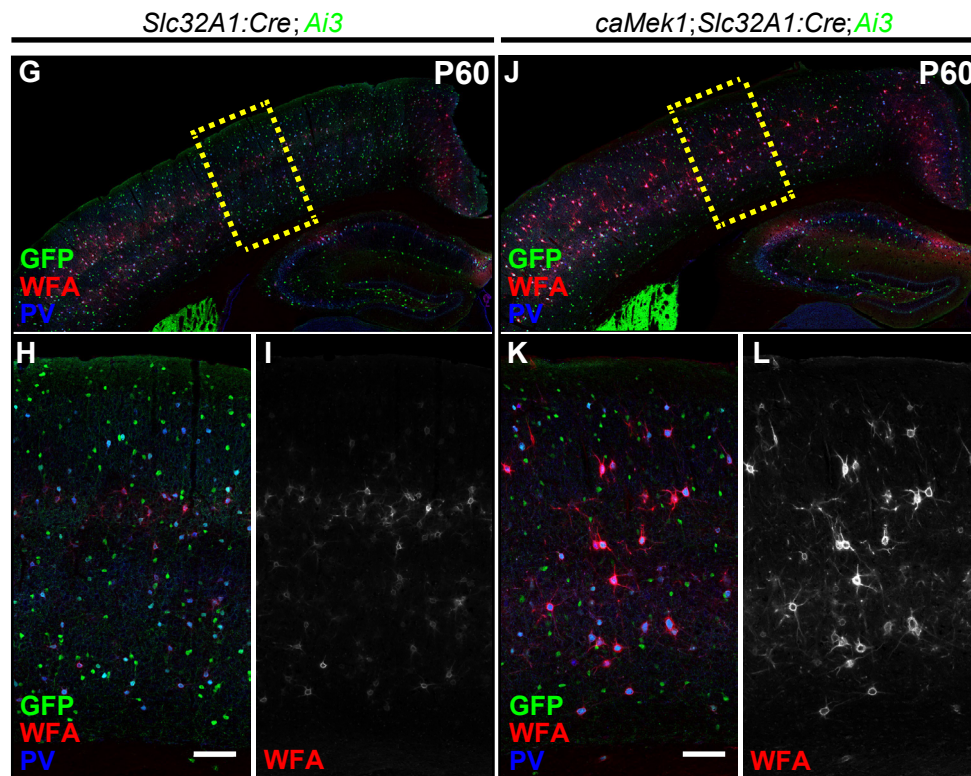
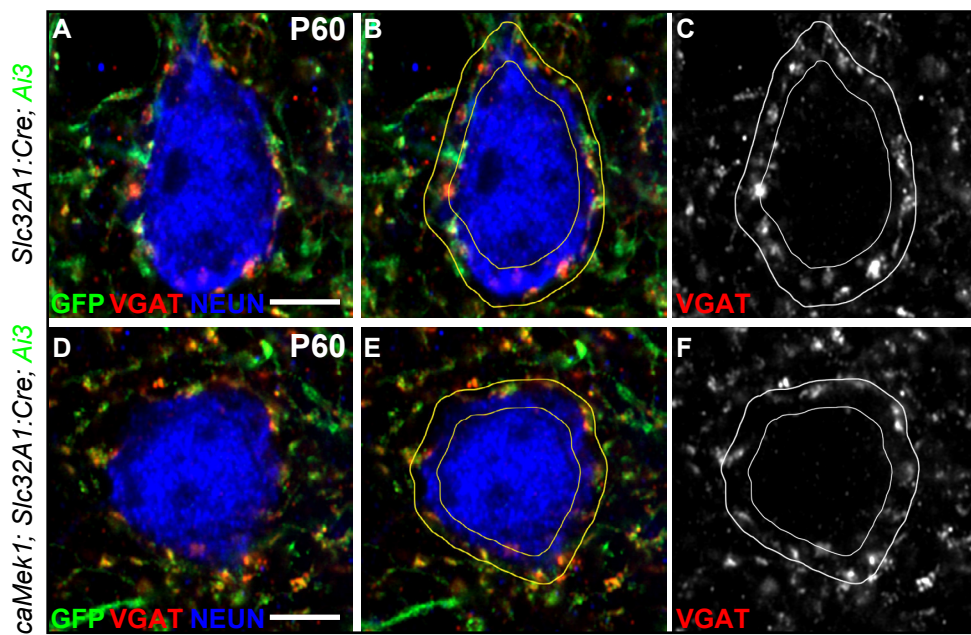
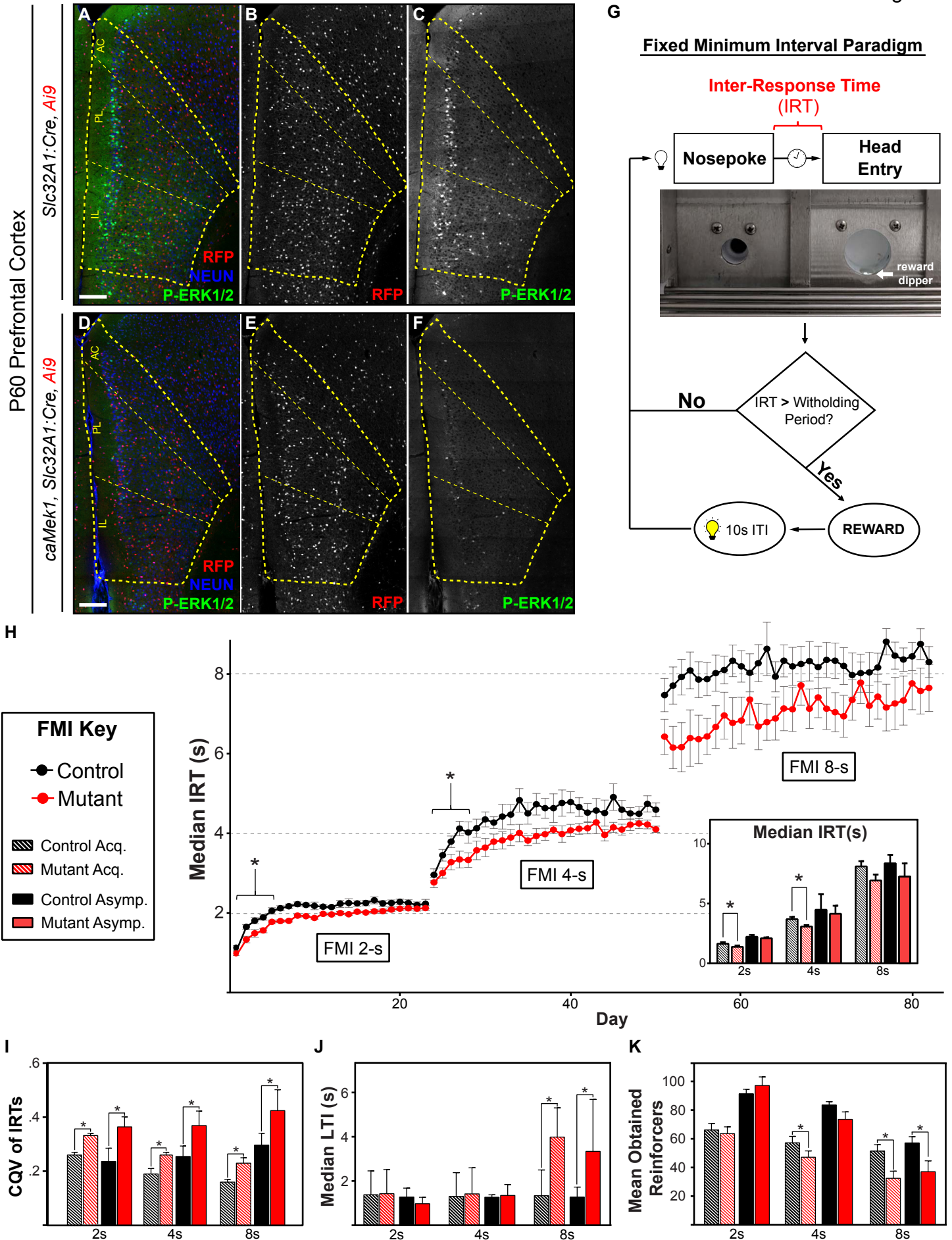


Figure 6



Supplemental Information

Table S1. Mouse Strains

Mouse Strain	Reference	Stock Number
<i>Nkx2.1-Cre</i>	Xu et al., 2008	Jax labs #008661
<i>Slc32A1-Cre</i>	Vong et al., 2011	Jax labs #028862
<i>Dlx5/6-Cre</i>	Monory et al., 2006	Jax labs #008199
<i>Map2k1^{S217/221E} (caMEK1)</i>	Krenz et al., 2008	
<i>Ai9</i> (Cre-dependent RFP)	Madisen et al., 2010	Jax labs #007909
<i>Ai3</i> (Cre-dependent GFP)	Madisen et al., 2010	Jax labs #007903

Table S2. Antibodies

Antibodies	Manufacturer	Catalog Number
Goat anti-Parvalbumin	Swant	PVG213
Rabbit anti-Somatostatin	Peninsula	T-4103
Biotinylated <i>Wisteria Floribunda Agglutinin</i>	Vector	B-1355
Chicken anti-GFP	Aves	GFP-1020
Chicken anti-RFP	Rockland	600-901-379
Rabbit anti-MEK1	Abcam	Ab32091
Rabbit anti-ERK2	Abcam	Ab32081
Rabbit anti-P-ERK1/2	Cell Signaling	4370
Mouse anti-NEUN	Millipore	Mab377
Rabbit anti-cleaved caspase 3	Cell Signaling	9664L
Rabbit anti-GFAP	Abcam	Ab7260
Rabbit anti-VGAT	Synaptic Systems	131 003
Mouse anti-8-oxo-dg	R&D Systems	4354-MC-050

Figure S1. Related to Figure 1

(A-H) Representative coronal sections of E13.5 developing mouse forebrain immunolabeled for MEK1. High expression of MEK1 was detected in RFP-labeled cells in *caMek1 Slc32A1:Cre* ganglionic eminences and CIN migratory streams (compare **C** to **G**; **D** to **H**). **(I)** *CaMek1 Slc32A1:Cre* mice exhibited significantly increased body mass in adulthood as compared to controls (n = 12 controls, 12 mutants; mean \pm SEM, * = $p < 0.05$). **(J-O)** Mutant CINs display increased MEK1 expression into adulthood (n=3). (Scale bar = 25 μ m)

Figure S2. Related to Figure 2

(A-D) P30 coronal sections of *caMek1 Dlx5/6:Cre* primary sensory cortex revealed a substantial qualitative decrease in the number of PV-CINs relative to controls (n=3). **(E-M)** Representative confocal images of P14 *caMek1 Nkx2.1:Cre* sensory cortices immunolabeled for PV. The number of PV⁺/RFP⁺ co-expressing cells was significantly decreased in mutants as compared to littermate controls (quantification in **M**: n = 3; mean \pm SEM, * = $p < 0.05$).

Figure S3. Related to Figure 3

(A-D) Representative confocal micrographs of the E17.5 developing cortical plate. A significant decrease in the number of RFP⁺ CINs was detected in *caMek1 Slc32A1:Cre* embryos (quantification in **E**: n = 3; mean \pm SEM, * = $p < 0.05$).

Figure S4. Related to Figure 4

(A-B) *CaMek1 Slc32A1:Cre* mice (n = 25 control, 13 mutant) were assessed for locomotor, anxiety-like behaviors, and sociability in the open field task. No significant differences in distance traveled or center time were observed throughout 10 min of open field testing. **(C-E)** Elevated plus maze testing did not detect a significant difference in % open arm entries or % time spent in open arms. **(F-H)** In the social

approach assay mutants did not significantly differ from controls in total entries, time spent in the social side, or social side entries.

Figure S5. Related to Figure 5

(A-E) Mutant mice exhibited normal VGAT-labeling in the layer 2/3 neuropil (quantification in **E**; n = 33 control, 30 mutant regions, mean \pm SEM). **(F-I)** Expression of the DNA oxidation marker 8-oxo-dg expression in WFA⁺ *caMek1 Slc32A1:Cre* CINs was qualitatively unchanged when compared to control WFA⁺ CINs (control in F-G, mutant in H-I). (Scale bar = 25 μ m).

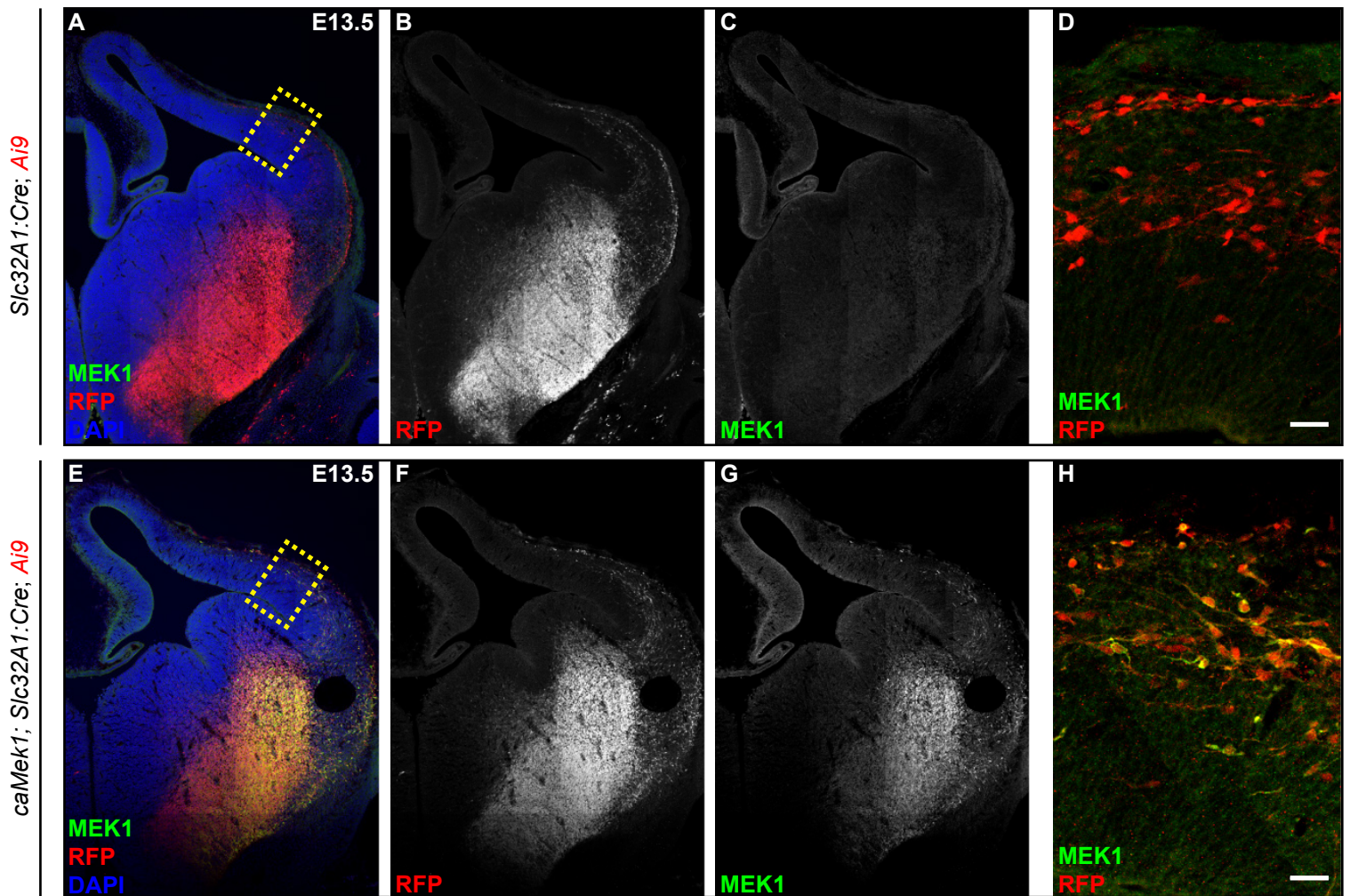
Supplemental Video 1.

Representative video montages of two control and two *caMek1 Slc32A1:Cre* mutants that showed abnormal rearing, neck twitching, and hypolocomotion during the first 60 seconds of the open field task.

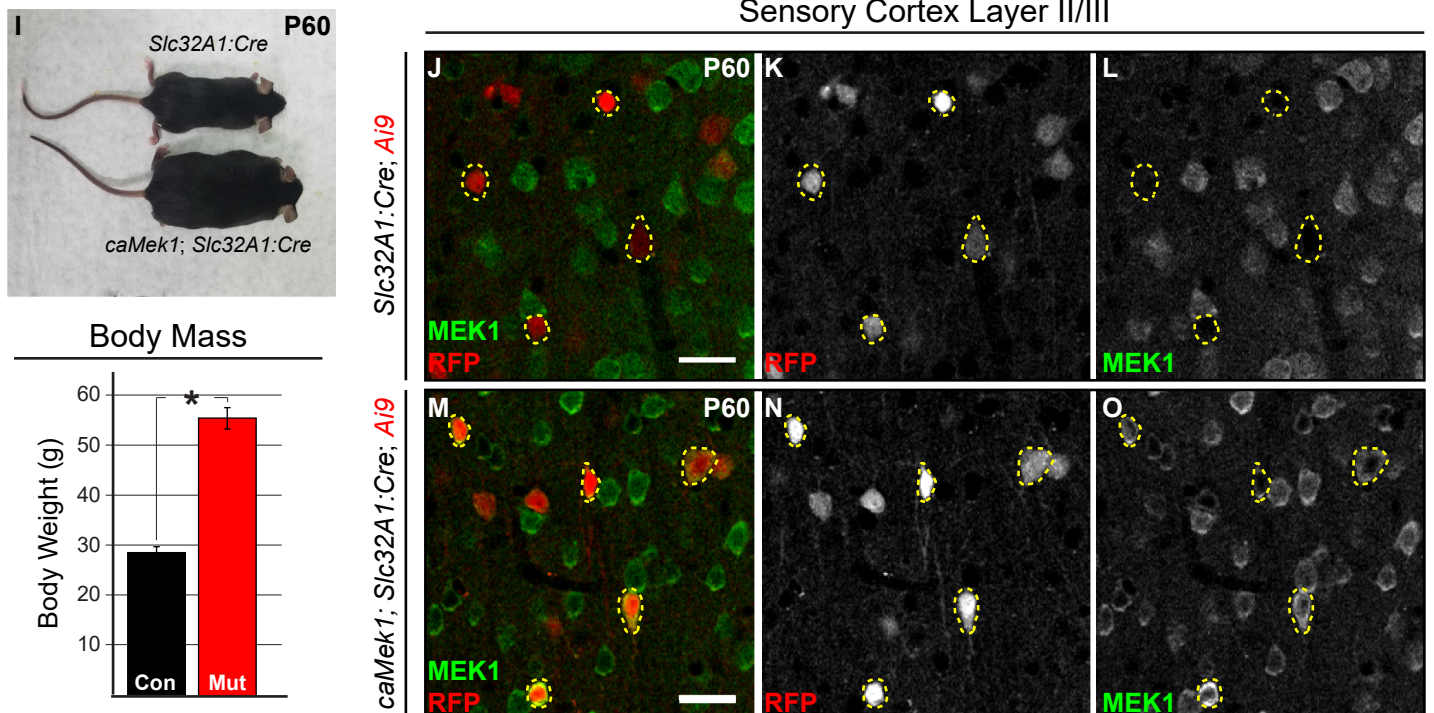
Supplemental Video 2.

Representative video montages of three control and three *caMek1 Slc32A1:Cre* mutants that underwent sudden behavioral arrest, abnormal head twitching, or motionless staring during the first 60 seconds of the open field task.

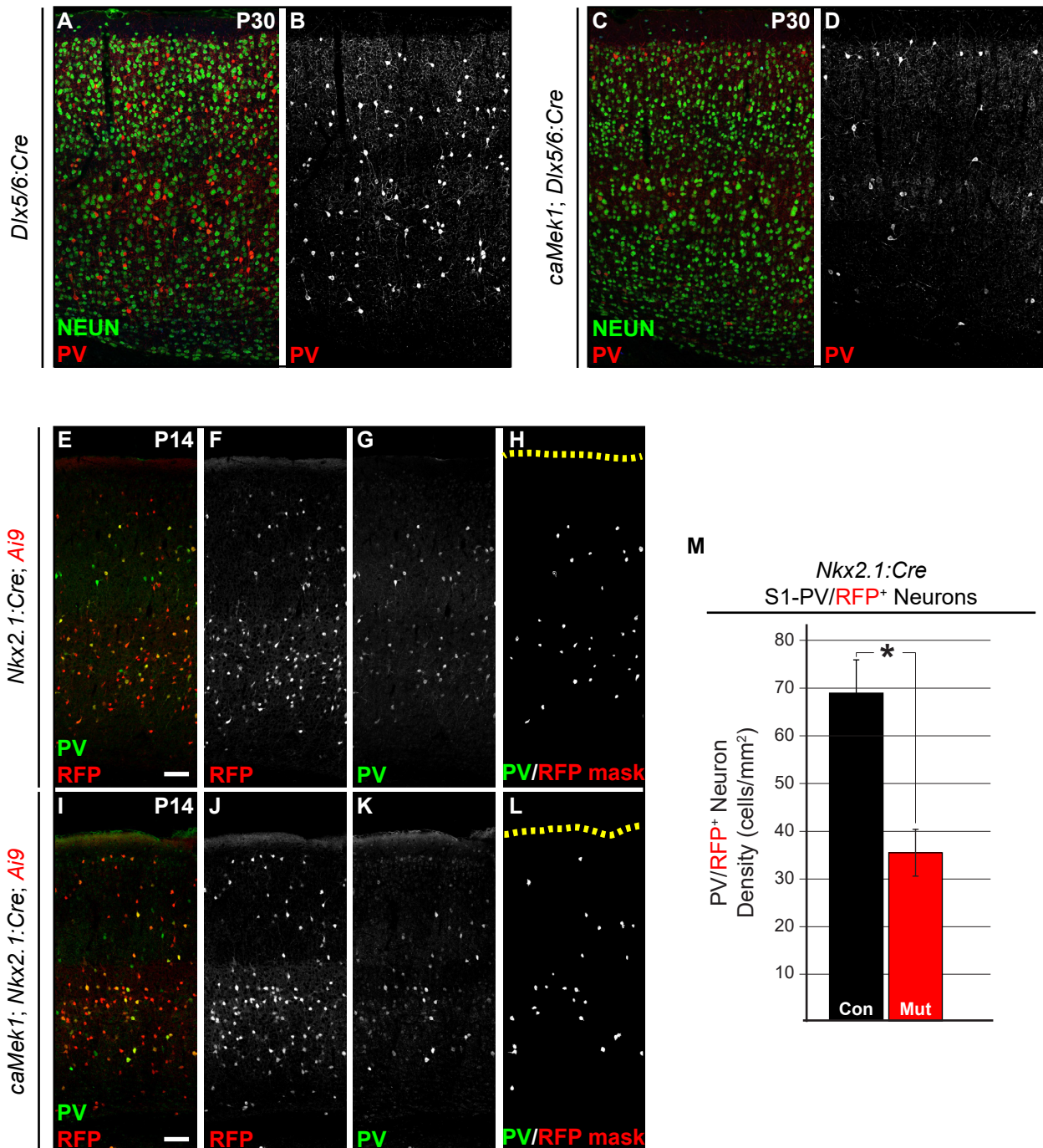
Developing Embryonic Forebrain



Sensory Cortex Layer II/III



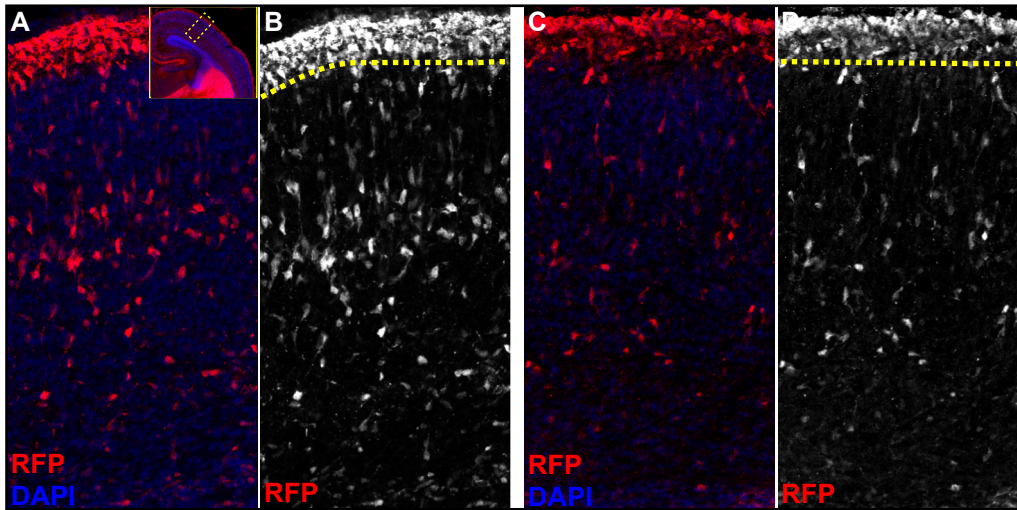
Primary Somatosensory Cortex



E17.5 Cortical Plate

Slc32A1:Cre; Ai9

caMek1; Slc32A1:Cre; Ai9



E

E17.5 Cortical Plate
GABAergic Neurons

